Discrete effects on the source term for the lattice Boltzmann modelling of one-dimensional reaction–diffusion equations

Goncalo Silva

IDMEC, Mechatronics Department, University of Évora, R. Romão Ramalho 59, 7000-671, Évora, Portugal

ARTICLE INFO

ABSTRACT

This work presents a detailed numerical analysis of one-dimensional, time-dependent (linear) reaction–diffusion type equations modelled with the lattice Boltzmann method (LBM), using the two-relaxation-time (TRT) scheme, for the D1Q3 lattice. The interest behind this study is twofold. First, because it applies to the description of many engineering problems, such as the mass transport in membranes, the heat conduction in fins, or the population growth in biological systems. Second, because this study also permits understanding the general effect of solution-dependent sources in LBM, where this problem offers a simple, yet non-trivial, canonical groundwork. Without recurring to perturbative techniques, such as the Chapman-Enskog expansion, we exactly derive the macroscopic numerical scheme that is solved by the LBM-TRT model with a solution-dependent source and show that it obeys a four-level explicit finite difference structure. In the steady-state limit, this scheme reduces to a second-order finite difference approximation of the stationary reaction–diffusion equation that, due to artefacts from the source term discretization, may operate with an effective diffusion coefficient of negative value, although still remaining stable. Such a surprising result is demonstrated through an exact stability analysis that proves the unconditional stability of the LBM-TRT model with a solution-dependent source, in line with the already proven source-less pure diffusion case (Lin et al., 2021). This proof enlarges the confidence over the LBM-TRT model robustness also for the (linear) reaction–diffusion problem class. Finally, a truncation error analysis is performed to disclose the structure of the leading order errors. From this knowledge, two strategies are proposed to improve the scheme accuracy from second- to fourth-order. One exclusively based on the tuning of the LBM-TRT scheme free-parameters, namely the two relaxation rates and the lattice weight coefficient, and the other based on the redefinition of the structure of the relaxation rates, where the leading order truncation error is absorbed into one of the relaxation rates, liberating the other to improve additional features of the scheme. Numerical tests presented in the last part of the work support the ensemble of theoretical findings.

1. Introduction

Consider the diffusive transport of mass, heat or any other scalar quantity, represented by the variable $\phi(x,t)$, which is simultaneously determined by: (i) the diffusion coefficient $\mathcal{D} > 0$, (ii) a first-order reaction term $-\kappa\,\phi(x,t)$, controlled by the reaction constant $\kappa \geq 0$, and (iii) a constant source term $\mathcal{M}$. This is a textbook problem [1] described by the following partial differential equation [2,3]:

$$\frac{\partial \phi}{\partial t} = \mathcal{D}\,\frac{\partial^2 \phi}{\partial x^2} - \kappa\,\phi + \mathcal{M}. \tag{1}$$

Eq. (1) represents a one-dimensional reaction–diffusion model and governs numerous physical processes; for example, the diffusive mass transport in membranes [4] or reactors [5], the heat conduction in extended surfaces [6] or domains with internal heat sources [7], the evolution of populations within biological systems [8], etc. Although Eq. (1) is solvable by analytical methods under a wide range of initial and boundary conditions [2,3], it is often more convenient to solve it numerically. First, because when solving Eq. (1), numerical methods generally tend to exhibit comparable accuracy to analytical ones, particularly, when the latter are described by infinite series solutions [9]. And, second, because reaction–diffusion models of the type shown in Eq. (1) tend to appear in the context of more complex physical systems, e.g. as part of coupled reaction–diffusion equations [10], conjugated with fluid flows equations [11], or linked with other multiphysics problems [12], where the only workable path to solving Eq. (1) is through numerical approximations.

When compared to the traditional diffusion equation [2,3], the modelling of the reaction–diffusion system, presented in Eq. (1), introduces

a solution-dependent source term as new numerical challenge. The relative strength of this source compared to the diffusion term is typically quantified by the Damköhler number, $\mathrm{Da} = \kappa \ell^2 / D$, where ℓ measures some physically characteristic length scale [2]. At large Da regimes, the reaction source tends to dominate the solution behaviour, which is important to consider both from physical and numerical viewpoints. So, while this $\mathrm{Da} \gg 1$ regime is where the source term needs to be more accurately modelled, it is, at the same time, the case where its numerical modelling is more challenging, which justifies the ongoing research on this topic [13].

This work concerns with the lattice Boltzmann method (LBM) [14–17] as numerical technique to solve Eq. (1). The LBM is a simple and versatile numerical approach that, when compared to classical numerical techniques, is able to reach very competitive standards in a variety of physical models [18–21], ranging from standard fluid flow [22,23] or advection–diffusion transport problems [24,25] to other types of partial differential equations [17,26,27], such as those described by the Poisson equation [28], Burgers–Fisher equation [29], Ginzburg–Landau equation [30], Schrödinger equation [31,32], Dirac equation [33,34], etc. In many of these instances, a space–time- or solution-dependent source is part of the governing equation. Therefore, the numerical analysis of LBM as solver to Eq. (1) also offers a valuable apparatus to study more general problem classes, such as those enumerated above, where an external source is present and plays a pivotal role.

The clean inclusion of external sources into the LBM equation has been the subject of many works [35–43]. In a nutshell, those studies shared a common objective: to derive a consistent formulation of the LBM external source term, which guarantees an artefact-free representation of this source at macroscopic level. Nowadays, after numerous and valuable contributions, it appears that a general understanding on this field has been reached [16]. Yet, in the author's opinion the topic remains far from closed, since most of the conclusions derived from those works develop upon asymptotic techniques, such as the Chapman-Enskog expansion [37,38] or similar ones [23,44,45], where the analysis is usually truncated to second order terms. Thus, at best, such works only unveil the LBM behaviour at the so-called "hydrodynamic limit" [46], a level of approximation that may hide important characteristics of the numerical method. To reach out a more complete picture of the LBM scheme, it is typically required considering the inclusion of higher-order terms in the analysis (to capture, at least, the leading truncation errors in the numerical approximation [47–51]) or, in the limit, even the exact full scheme written at discrete level [42,47, 52–55]. Unfortunately, apart from a few exceptions [42,52,53,55], the publication of truncation error analyses to study the discrete effects on the LBM source term has been very scarce. The attempt to fill this gap is, therefore, a purpose of the present study.

Historically, one of the earliest efforts to characterize LBM, in relation to conventional numerical methods, was due to Ancona [56], which pointed out the similitude between the D1Q2 lattice structure and the DuFort-Frankel scheme [9] for 1D convection–diffusion equations. Later, He et al. [57] focused on simple, steady and unidirectional fluid flow problems, taking place in channels, to demonstrate that the LBM discrete structure in bulk is equivalent to a second-order central difference approximation of the incompressible Navier–Stokes equations. This methodology was further extended to the assessment of other discrete features of the LBM scheme, such as the origin of the spurious slip on boundary conditions [58,59] or the discrete lattice artefacts due to external forcing terms [42,52,53,55,60]. Complementary efforts on the understanding of LBM as a numerical scheme focused on the study of its truncation structure, by delving into third- and higher-order asymptotic analyses [49–51,61]. In this regard, a key contribution was due to Holdych et al. [62] who revealed that the LBM truncation errors followed a rather organized structure, with its single relaxation time parameter obeying, at each order, a well-defined hierarchy built upon functioned polylogarithm polynomials [63]. Such

a result was later verified by many other independent studies, recurring to diverse asymptotic techniques, such as the Chapman-Enskog expansion [47], Maxwell iteration [44], direct Taylor expansion [61], recurrence equations [47,54], etc. Their application to the study of external source terms has been also reported [64], although typically limited to a third-order truncation analysis. The linkage between the discrete level studies and the truncation error analyses has been established by Ginzburg and co-workers in a series of valuable contributions [47,48,53,54]. Of particular importance to the present study is the work [47], which examined the discrete and truncation structure of the equations satisfied by the LBM two-relaxation-time approximation of convection–diffusion equations, and the works [53,65], which analysed and improved the body force discrete lattice effects arising in the LBM-Brinkman modelling of steady flows in porous media; the application of this analysis to other types of steady flow problems was recently given in [42].

In spite of the valuable works listed above, some important questions regarding the discrete and truncation structure of the LBM subject to external sources remain to be answered, namely: (i) What is the finite difference representation of the LBM source term in a time-dependent setting? (ii) How is the LBM scheme able to converge in a stable manner towards a steady-state solution, even when its effective diffusion coefficient becomes negative due to source term discretization artefacts? (iii) How does the external source inclusion alters the leading-order truncation structure of the LBM scheme and how does its effect can be mitigated in order to improve the accuracy and quality of the numerical solutions? This work intends to answer these questions by studying the LBM approximation of Eq. (1). For this task, the two-relaxation-time (TRT) collision model on the D1Q3 lattice is considered, which gives access to the exact analytical solutions of the scheme, while being extendable to higher dimensions by taking tensor-products of this lattice. Therefore, on top of the fundamental insight obtained here, the present study is also expected to provide a useful groundwork to guide in the development of improved LBM models for larger scale reaction–diffusion applications, as those reported in [66–71].

The rest of this paper is organized as follows. Section 2 introduces the LBM-TRT basic equations and the nomenclature adopted in this work. Section 3 derives the explicit multi-level finite-difference scheme satisfied by the LBM-TRT model in approximating Eq. (1); the steady-state regime is also discussed at the end of this section. Section 4 demonstrates the unconditional stability of the LBM-TRT scheme with a source, for any Damköhler number, Da, for the parameters that appear in the scheme. Section 5 presents a truncation error analysis, with focus on the optimal values of the LBM free parameters that permit increasing the scheme accuracy and then on the development of an improved strategy, inspired in [65], that mitigates the external source term artefacts. Section 6 shows numerical simulations performed on four benchmarks tests, which confirm the study theoretical conclusions. Finally, Section 7 concludes the work with a summary of the main results.

2. Lattice Boltzmann method with a source term

The LBM-TRT [39,47,54] representation of Eq. (1) can be obtained by solving for the populations $f_q(x_j, t_n)$, defined on discrete space x_j and the discrete time t_n, along the discrete velocity set $\mathbf{c}_q$, featuring one immobile $\mathbf{c}_0 = \mathbf{0}$ and $Q - 1$ non-zero velocity vectors $\mathbf{c}_q$ per grid node. The TRT collision model is formulated on the symmetry argument that any lattice quantity ψ_q can be decomposed onto symmetric $\psi_q^+ = \frac{1}{2}(\psi_q + \psi_{\bar{q}})$ and anti-symmetric $\psi_q^- = \frac{1}{2}(\psi_q - \psi_{\bar{q}})$ components, where $\mathbf{c}_{\bar{q}} = -\mathbf{c}_q$. The evolution equation of the LBM-TRT scheme, under equilibrium $e_q(x_j, t_n)$ and external source term $M_q(x_j, t_n)$, can be written

as:

$$
\begin{aligned}
f_q(x_j + \mathbf{c}_q\,\Delta t, t_n + \Delta t) =\; & f_q(x_j, t_n) - s^+ \left(f_q^+(x_j, t_n) - e_q^+(x_j, t_n) \right) \\
& - s^- \left(f_q^-(x_j, t_n) - e_q^-(x_j, t_n) \right) \\
& + \Delta t \left(1 - \frac{s^+}{2} \right) M_q^+(x_j, t_n) \\
& + \Delta t \left(1 - \frac{s^-}{2} \right) M_q^-(x_j, t_n).
\end{aligned} \tag{2}
$$

In D1Q3 lattice [16] the index $q = \{-1, 0, 1\}$ and the discrete velocity vector $\mathbf{c}_q$ reads:

$$
\mathbf{c}_q = \begin{cases} -c, & q = -1, \\ 0, & q = 0, \\ c, & q = 1, \end{cases} \tag{3}
$$

where $c = \Delta x / \Delta t$, with Δx and Δt the space and time step increment, respectively.

The D1Q3 lattice weight coefficients ω_q follow an isotropic structure, given by:

$$
\omega_1 = \omega_{-1} = \frac{1 - \omega_0}{2}. \tag{4}
$$

The resting weight ω_0 is a free-tunable parameter, constrained to the necessary stability range $0 < \omega_0 < 1$ [47,72]. These weights satisfy the constraints $\omega_q > 0 \; \forall \, q$ and $\sum_q \omega_q = 1$.

The LBM-TRT model, Eq. (2) approximates the macroscopic diffusion equation, Eq. (1), with the following equilibrium populations:

$$
e_q^+(x_j, t_n) = \omega_q\, \phi(x_j, t_n) \quad \text{and} \quad e_q^-(x_j, t_n) = 0, \tag{5}
$$

where ϕ is the macroscopic variable of interest.

The first three velocity moments of the equilibrium produces the following results:

$$
\begin{aligned}
& \sum_q e_q^+(x_j, t_n) = \phi(x_j, t_n), \quad \sum_q \mathbf{c}_q\, e_q^-(x, t) = \mathbf{0}, \\
& \sum_q \mathbf{c}_q^2\, e_q^+(x_j, t_n) = \left(1 - \omega_0 \right) \phi(x_j, t_n)\, c^2.
\end{aligned} \tag{6}
$$

The discrete source term is:

$$
M_q^+(x_j, t_n) = \omega_q \left(-\kappa\, \phi(x_j, t_n) + \mathcal{M} \right) \quad \text{and} \quad M_q^-(x_j, t_n) = 0. \tag{7}
$$

The macroscopic variable $\phi(x_j, t_n)$ is found through the LBM-TRT solution $f_q(x_j, t_n)$ as follows

$$
\begin{aligned}
& \phi(x_j, t_n) = \sum_q f_q(x_j, t_n) + \frac{\Delta t}{2} \left(-\kappa\, \phi(x_j, t_n) + \mathcal{M} \right) \\
& \Rightarrow \quad \left(1 + \kappa\, \frac{\Delta t}{2} \right) \phi(x_j, t_n) = \sum_q f_q(x_j, t_n) + \frac{\Delta t}{2} \mathcal{M}.
\end{aligned} \tag{8}
$$

The TRT collision is controlled by two relaxation rates $s^\pm \in\,]0, 2[$, where the even-order relaxation rate s^+ is free-tunable, and the odd-order relaxation rate s^- is related to the diffusion coefficient D in Eq. (1), as:

$$
D = (1 - \omega_0) \left(\frac{1}{s^-} - \frac{1}{2} \right) \frac{\Delta x^2}{\Delta t}. \tag{9}
$$

Finally, it is convenient to define the following TRT relaxation functions:

$$
\Lambda^\pm = \left(\frac{1}{s^\pm} - \frac{1}{2} \right), \quad \text{and} \quad \Lambda = \Lambda^+ \Lambda^-. \tag{10}
$$

3. Difference equations of LBM-TRT reaction–diffusion model

3.1. Time-dependent difference scheme

This section derives the equivalent finite difference structure of the LBM-TRT model presented in Section 1. This derivation tightly

follows the works [73–75]. To simplify notation, we introduce the grid coordinate system $x_j = j\,\Delta x$ and $t_n = n\,\Delta t$ and define $f_{q,j}^n := f_q(j\,\Delta x, n\,\Delta t)$ and $\phi_j^n := \phi(j\,\Delta x, n\,\Delta t)$. By substituting the equilibrium distribution function, Eq. (5), and the discrete source term, Eq. (7), into the LBM-TRT evolution equation, Eq. (2), we can write the explicit form of each population within the D1Q3 model as follows:

$$
\begin{aligned}
f_{-1,j}^{n+1} =\; & f_{-1,j+1}^n - \frac{s^-}{2} \left(f_{-1,j+1}^n - f_{1,j+1}^n \right) + \frac{s^+}{2} f_{0,j+1}^n \\
& - \left[\frac{\omega_0\, s^+}{2} + \kappa\, \Delta t \left(\frac{1-\omega_0}{2} + \frac{\omega_0\, s^+}{4} \right) \right] \phi_{j+1}^n + \left(\frac{1-\omega_0}{2} + \frac{\omega_0\, s^+}{4} \right) \Delta t\, \mathcal{M},
\end{aligned} \tag{11a}
$$

$$
\begin{aligned}
f_{0,j}^{n+1} =\; & f_{0,j}^n - s^+ f_{0,j}^n + \left[\omega_0\, s^+ - \kappa\, \Delta t\, \omega_0 \left(1 - \frac{s^+}{2} \right) \right] \phi_j^n \\
& + \omega_0 \left(1 - \frac{s^+}{2} \right) \Delta t\, \mathcal{M},
\end{aligned} \tag{11b}
$$

$$
\begin{aligned}
f_{1,j}^{n+1} =\; & f_{1,j-1}^n + \frac{s^-}{2} \left(f_{-1,j-1}^n - f_{1,j-1}^n \right) + \frac{s^+}{2} f_{0,j-1}^n \\
& - \left[\frac{\omega_0\, s^+}{2} + \kappa\, \Delta t \left(\frac{1-\omega_0}{2} + \frac{\omega_0\, s^+}{4} \right) \right] \phi_{j-1}^n + \left(\frac{1-\omega_0}{2} + \frac{\omega_0\, s^+}{4} \right) \Delta t\, \mathcal{M}.
\end{aligned} \tag{11c}
$$

Inserting Eqs. (11) into Eq. (8), taking into account $\left(1 + \kappa\, \frac{\Delta t}{2} \right) \phi_j^{n+1} = f_{-1,j}^{n+1} + f_{0,j}^{n+1} + f_{1,j}^{n+1} + \frac{\Delta t}{2} \mathcal{M}$, we obtain:

$$
\begin{aligned}
\left(1 + \kappa\, \frac{\Delta t}{2} \right) \phi_j^{n+1} =\; & \left(f_{-1,j+1}^n + f_{0,j}^n + f_{1,j-1}^n \right) - \frac{s^-}{2} \left[\left(f_{-1,j+1}^n - f_{1,j+1}^n \right) \right. \\
& \left. - \left(f_{-1,j-1}^n - f_{1,j-1}^n \right) \right] \\
& + \frac{s^+}{2} \left(f_{0,j+1}^n - 2 f_{0,j}^n + f_{0,j-1}^n \right) \\
& - \frac{\omega_0\, s^+}{2} \left(\phi_{j+1}^n - 2 \phi_j^n + \phi_{j-1}^n \right) \\
& - \kappa\, \Delta t \left(\frac{1-\omega_0}{2} + \frac{\omega_0\, s^+}{4} \right) \left(\phi_{j+1}^n + \phi_{j-1}^n \right) \\
& - \kappa\, \Delta t \left(\omega_0 - \frac{\omega_0\, s^+}{2} \right) \phi_j^n + \frac{3}{2} \Delta t\, \mathcal{M}.
\end{aligned} \tag{12}
$$

The focus now will be dedicated to simplifying the first three terms on the right-hand side of Eq. (12), replacing the mesoscopic populations f_q by the macroscopic variable ϕ.

The first term on the right-hand side of Eq. (12) can be simplified by summing Eq. (8) at points $j + 1$ and $j - 1$ (both at time step n), and then using $f_{1,j+1}^n + f_{0,j}^n + f_{-1,j-1}^n = \left(1 - \kappa\, \frac{\Delta t}{2} \right) \phi_j^{n-1} + \frac{\Delta t}{2} \mathcal{M}$, which will result in:

$$
\begin{aligned}
f_{-1,j+1}^n + f_{0,j}^n + f_{1,j-1}^n =\; & - \left(f_{0,j+1}^n - 2 f_{0,j}^n + f_{0,j-1}^n \right) \\
& + \left(\phi_{j+1}^n + \phi_{j-1}^n - \phi_j^{n-1} \right) \\
& + \kappa\, \frac{\Delta t}{2} \left(\phi_{j+1}^n + \phi_{j-1}^n + \phi_j^{n-1} \right) - \frac{3}{2} \Delta t\, \mathcal{M}.
\end{aligned} \tag{13}
$$

The second term on the right-hand side of Eq. (12) can be simplified through a similar procedure, which permits obtaining:

$$
\begin{aligned}
\left(f_{-1,j+1}^n - f_{1,j+1}^n \right) - \left(f_{-1,j-1}^n - f_{1,j-1}^n \right) =\; & - \left(f_{0,j+1}^n - 2 f_{0,j}^n + f_{0,j-1}^n \right) \\
& + \left(\phi_{j+1}^n + \phi_{j-1}^n - 2 \phi_j^{n-1} \right) \\
& + \kappa\, \frac{\Delta t}{2} \left(\phi_{j+1}^n + \phi_{j-1}^n + 2 \phi_j^{n-1} \right) \\
& - 2\, \Delta t\, \mathcal{M}.
\end{aligned} \tag{14}
$$

The introduction of Eqs. (13) and (14) into Eq. (12) will lead to:

$$
\begin{aligned}
\left(1 + \kappa \frac{\Delta t}{2}\right) \phi_j^{n+1} = & \left(\frac{s^-}{2} + \frac{s^+}{2} - 1\right)\left(f_{0,j+1}^n - 2 f_{0,j}^n + f_{0,j-1}^n\right) \\
& + \left(1 - \frac{s^-}{2} - \frac{\omega_0 s^+}{2}\right)\left(\phi_{j+1}^n + \phi_{j-1}^n\right) + \omega_0 s^+ \phi_j^n \\
& + (s^- - 1)\phi_j^{n-1} \\
& - \kappa \Delta t \left(\frac{\omega_0 s^+}{4} + \frac{s^-}{4} - \frac{\omega_0}{2}\right)\left(\phi_{j+1}^n + \phi_{j-1}^n\right) \\
& - \kappa \Delta t \left(\omega_0 - \frac{\omega_0 s^+}{2}\right)\phi_j^n - \kappa \frac{\Delta t}{2}(s^- - 1)\phi_j^{n-1} \\
& + s^- \Delta t \, \mathcal{M}.
\end{aligned}
\tag{15}
$$

Now, we need to evaluate the first term on the right-hand side of Eq. (15). By introducing Eq. (8) and Eqs. (11) into $\left(f_{0,j+1}^n - 2 f_{0,j}^n + f_{0,j-1}^n\right)$, and then using $f_{1,j+1}^n + f_{0,j}^n + f_{-1,j-1}^n = \left(1 - \kappa \frac{\Delta t}{2}\right)\phi_j^{n-1} + \frac{\Delta t}{2}\mathcal{M}$, we will obtain:

$$
\begin{aligned}
f_{0,j+1}^n - 2 f_{0,j}^n + f_{0,j-1}^n = & (s^- - 1)\left(f_{0,j+1}^{n-1} - 2 f_{0,j}^{n-1} + f_{0,j-1}^{n-1}\right) \\
& - 2\phi_j^n + (2 - s^-)\left(\phi_{j+1}^{n-1} + \phi_{j-1}^{n-1}\right) \\
& + (2 s^- - 2)\phi_j^{n-2} \\
& - \kappa \Delta t \, \phi_j^n - \kappa \Delta t \frac{s^-}{2}\left(\phi_{j+1}^{n-1} + \phi_{j-1}^{n-1}\right) \\
& - \kappa \Delta t (s^- - 1)\phi_j^{n-2} \\
& + 2 s^- \Delta t \, \mathcal{M}.
\end{aligned}
\tag{16}
$$

Finally, by introducing Eq. (16) into Eq. (15), and recursively simplifying the result by re-introducing Eq. (15), this time re-expressed at time step $n - 1$, we obtain:

$$
\begin{aligned}
\left(1 + \kappa \frac{\Delta t}{2}\right) \phi_j^{n+1} = & \left(1 - \frac{s^-}{2} - \frac{\omega_0 s^+}{2}\right)\left(\phi_{j+1}^n + \phi_{j-1}^n\right) \\
& + (\omega_0 s^+ - s^+ + 1)\phi_j^n \\
& + \left(\frac{\omega_0 s^- s^+}{2} - \frac{\omega_0 s^+}{2} - \frac{s^- s^+}{2} + s^+ + \frac{s^-}{2} - 1\right) \\
& \times \left(\phi_{j+1}^{n-1} + \phi_{j-1}^{n-1}\right) \\
& + (-\omega_0 s^- s^+ + \omega_0 s^+ + s^- - 1)\phi_j^{n-1} \\
& + (s^- s^+ - s^+ - s^- + 1)\phi_j^{n-2} \\
& - \kappa \Delta t \left(\frac{\omega_0 s^+}{4} + \frac{s^-}{4} - \frac{\omega_0}{2}\right)\left(\phi_{j+1}^n + \phi_{j-1}^n\right) \\
& - \kappa \Delta t \left(-\frac{\omega_0 s^+}{2} + \frac{s^+}{2} + \omega_0 - \frac{1}{2}\right)\phi_j^n \\
& - \kappa \Delta t \left(-\frac{\omega_0 s^- s^+}{4} + \frac{\omega_0 s^+}{4}\right. \\
& \left. + \frac{\omega_0 s^-}{2} + \frac{s^+ s^-}{4} - \frac{s^-}{4} - \frac{\omega_0}{2}\right)\left(\phi_{j+1}^{n-1} + \phi_{j-1}^{n-1}\right) \\
& - \kappa \Delta t \left(\frac{\omega_0 s^- s^+}{2} - \frac{\omega_0 s^+}{2} - \omega_0 s^-\right. \\
& \left. + \frac{s^-}{2} + \omega_0 - \frac{1}{2}\right)\phi_j^{n-1} \\
& - \kappa \Delta t \left(\frac{s^- s^+}{2} - \frac{s^+}{2} - \frac{s^-}{2} + \frac{1}{2}\right)\phi_j^{n-2} + s^- s^+ \Delta t \, \mathcal{M}.
\end{aligned}
\tag{17}
$$

Eq. (17) can be written in compact form as follows:

$$
\begin{aligned}
\phi_j^{n+1} = & \alpha_1 \phi_{j-1}^n + \alpha_2 \phi_j^n + \alpha_1 \phi_{j+1}^n + \beta_1 \phi_{j-1}^{n-1} \\
& + \beta_2 \phi_j^{n-1} + \beta_1 \phi_{j+1}^{n-1} + \gamma \phi_j^{n-2} + \zeta \mathcal{M},
\end{aligned}
\tag{18}
$$

with coefficients

$$
\begin{aligned}
\alpha_1 := & \frac{2}{2 + \kappa \Delta t}\left[\left(-\frac{s^-}{2} + 1 - \omega_0 \frac{s^+}{2}\right) - \kappa \frac{\Delta t}{2}\left(\frac{s^-}{2} + \omega_0\left(\frac{s^+}{2} - 1\right)\right)\right] \\
\alpha_2 := & \frac{2}{2 + \kappa \Delta t}\left[(-s^+ + 1 + \omega_0 s^+) - \kappa \frac{\Delta t}{2}\left(s^+ - 1 + \omega_0(-s^+ + 2)\right)\right] \\
\beta_1 := & \frac{2}{2 + \kappa \Delta t}\left[\left(-\frac{s^- s^+}{2} + s^+ + \frac{s^-}{2} - 1 + \omega_0\left(\frac{s^- s^+}{2} - \frac{s^+}{2}\right)\right)\right. \\
& \left. - \kappa \frac{\Delta t}{2}\left(\frac{s^+ s^-}{2} - \frac{s^-}{2} + \omega_0\left(-\frac{s^- s^+}{2} + \frac{s^+}{2} + s^- - 1\right)\right)\right] \\
\beta_2 := & \frac{2}{2 + \kappa \Delta t}\left[\left(s^- - 1 + \omega_0(-s^- s^+ + s^+)\right)\right. \\
& \left. - \kappa \frac{\Delta t}{2}\left(-1 + s^- + \omega_0\left(s^- s^+ - s^+ - 2 s^- + 2\right)\right)\right] \\
\gamma := & \frac{2}{2 + \kappa \Delta t}\left[(s^- - 1)(s^+ - 1) - \kappa \frac{\Delta t}{2}(s^- - 1)(s^+ - 1)\right] \\
\zeta := & \frac{2}{2 + \kappa \Delta t}\Delta t \, s^- s^+
\end{aligned}
\tag{19}
$$

or, alternatively, by considering the TRT relaxation parameters $\Lambda^\pm = \left(\frac{1}{s^\pm} - \frac{1}{2}\right)$ and $\Lambda = \Lambda^+ \Lambda^-$, defined in Eq. (10), where $s^+ s^- = \left(\Lambda + \frac{\Lambda^+ + \Lambda^-}{2} + \frac{1}{4}\right)^{-1}$, the coefficients in Eq. (19) may be re-written in the following form:

$$
\begin{aligned}
\alpha_1 := & \frac{2 s^+ s^-}{2 + \kappa \Delta t}\left[\left(\Lambda - \frac{1}{4} + (1 - \omega_0)\left(\frac{\Lambda^-}{2} + \frac{1}{4}\right)\right)\right. \\
& \left. - \kappa \frac{\Delta t}{2}\left(-\Lambda + \frac{1}{4} + (1 - \omega_0)\left(\Lambda + \frac{\Lambda^+}{2}\right)\right)\right] \\
\alpha_2 := & \frac{2 s^+ s^-}{2 + \kappa \Delta t}\left[\left(\Lambda + \frac{\Lambda^+ + \Lambda^-}{2} + \frac{1}{4} - (1 - \omega_0)\left(\Lambda^- + \frac{1}{2}\right)\right)\right. \\
& \left. - \kappa \frac{\Delta t}{2}\left(\Lambda + \frac{\Lambda^+ + \Lambda^-}{2} + \frac{1}{4} - (1 - \omega_0)\left(2\Lambda + \Lambda^+\right)\right)\right] \\
\beta_1 := & \frac{2 s^+ s^-}{2 + \kappa \Delta t}\left[\left(-\Lambda + \frac{1}{4} + (1 - \omega_0)\left(\frac{\Lambda^-}{2} - \frac{1}{4}\right)\right)\right. \\
& \left. - \kappa \frac{\Delta t}{2}\left(-\Lambda + \frac{1}{4} + (1 - \omega_0)\left(\Lambda - \frac{\Lambda^+}{2}\right)\right)\right] \\
\beta_2 := & \frac{2 s^+ s^-}{2 + \kappa \Delta t}\left[\left(-\Lambda + \frac{\Lambda^+ + \Lambda^-}{2} - \frac{1}{4} - (1 - \omega_0)\left(\Lambda^- - \frac{1}{2}\right)\right)\right. \\
& \left. - \kappa \frac{\Delta t}{2}\left(\Lambda - \frac{\Lambda^+ + \Lambda^-}{2} + \frac{1}{4} - (1 - \omega_0)\left(2\Lambda - \Lambda^+\right)\right)\right] \\
\gamma := & \frac{2 s^+ s^-}{2 + \kappa \Delta t}\left[\left(\Lambda - \frac{\Lambda^+ + \Lambda^-}{2} + \frac{1}{4}\right) - \kappa \frac{\Delta t}{2}\left(\Lambda - \frac{\Lambda^+ + \Lambda^-}{2} + \frac{1}{4}\right)\right] \\
\zeta := & \frac{2 s^+ s^-}{2 + \kappa \Delta t}\Delta t
\end{aligned}
\tag{20}
$$

Eq. (18) reveals that the LBM-TRT model, Eq. (2) approximates the one-dimensional reaction–diffusion equation, Eq. (1), as a fourth-level explicit finite difference scheme. The stencil structure of Eq. (18) is depicted in Fig. 1. Interestingly, the space–time discretization of the diffusion term and the source term follow a similar non-local and multi-level structure. The discretization of each term only differs in the coefficient values.

To conclude this section, we point out that the above results are consistent with previously published studies [73–75]. Namely, taking into account that, for the D1Q3 lattice, TRT and MRT collision models produce exactly identical macroscopic equations [72], if we consider a pure diffusion case, $\kappa = 0$, and set $s^- = s_1$ and $s^+ = s_2$ then our Eq. (17) recovers Eq. (21) from the work [75], derived for the MRT model. Alternatively, if we consider $\kappa = 0$ and $s^+ = s^- = s$ into Eq. (17), we recover Eq. (10) with coefficients Eq. (11) and Eq. (12) from the work [73], which were derived for the LBM-BGK model. Similarly, the LBM-REG model [75] is recovered for $s^+ = 1$ and $s^- = s$, whereas the LBM-LKS model [75] is obtained for $s^+ = s$ and $s^- = \frac{s}{1 - s\eta}$, where η is an adjusting parameter.
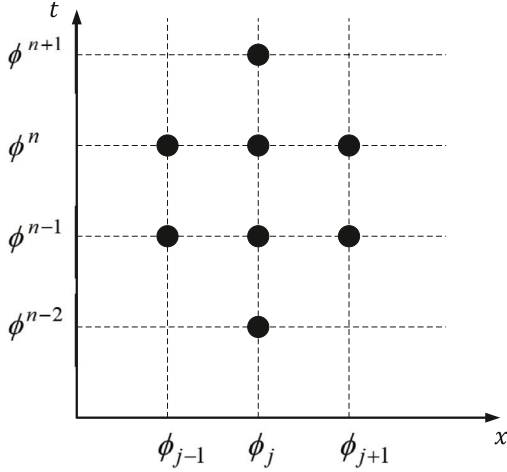
Fig. 1. Stencil of the difference scheme obeyed by the LBM-TRT on the D1Q3 lattice for the time-dependent reaction–diffusion equation.

3.2. Steady-state difference scheme

This section will study the steady state limit of Eq. (18).

3.2.1. Standard source scheme

For the time-independent regime, we drop the index n from the ϕ variable, multiply each term by $1/(\Delta t\, s^-\, s^+)$, and simplify the resulting equation to obtain:

$$(1 - \omega_0)\left(\frac{1}{s^-} - \frac{1}{2}\right)\frac{\Delta x^2}{\Delta t}\frac{\phi_{j-1} - 2\,\phi_j + \phi_{j+1}}{\Delta x^2} - \kappa\,\phi_j + \mathcal{M}$$
$$+ \left[\omega_0\left(\frac{1}{s^-} - \frac{1}{2}\right)\left(\frac{1}{s^+} - \frac{1}{2}\right) - \frac{1}{4}\right]\Delta x^2\,\kappa\,\frac{\phi_{j-1} - 2\,\phi_j + \phi_{j+1}}{\Delta x^2} = 0. \tag{21}$$

Eq. (21) can be simplified by introducing the following compact notation, namely: (i) the transport coefficient $\mathcal{D} = (1 - \omega_0)\left(\frac{1}{s^-} - \frac{1}{2}\right)\frac{\Delta x^2}{\Delta t}$, defined in Eq. (9), (ii) the TRT relaxation parameter $\Lambda := \left(\frac{1}{s^-} - \frac{1}{2}\right)\left(\frac{1}{s^+} - \frac{1}{2}\right)$, given in Eq. (10), and (iii) the discrete Laplacian operator given by $\bar{\Delta}_x^2 \phi_j := \frac{\phi_{j+1} - 2\,\phi_j + \phi_{j-1}}{\Delta x^2}$, which permits re-writing Eq. (21) in condensed form as:

$$\mathcal{D}\,\bar{\Delta}_x^2 \phi_j - \kappa\,\phi_j + \mathcal{M} + \left(\omega_0\,\Lambda - \frac{1}{4}\right)\Delta x^2\,\kappa\,\bar{\Delta}_x^2 \phi_j = 0. \tag{22}$$

If we assign to the free parameter ω_0 the hydrodynamic weight value $\omega_0 = \frac{2}{3}$, then Eq. (22) becomes:

$$\mathcal{D}\,\bar{\Delta}_x^2 \phi_j + \mathcal{M} - \kappa\left(\phi_j + \left(\frac{3 - 8\,\Lambda}{12}\right)\Delta x^2\,\bar{\Delta}_x^2 \phi_j\right) = 0. \tag{23}$$

Eq. (23) displays the discrete structure established by the LBM-TRT scheme when modelling the stationary reaction–diffusion equation, i.e. Eq. (1) with $\frac{\partial \phi}{\partial t} = 0$. It is interesting to note that this discrete structure is similar to the LBM-TRT modelling of (Brinkman-force) fluid flow problems in channel-like geometries [20,42,53,65], which hints to the universal structure of Eq. (23) in problems with solution-dependent source. Eq. (23) is the second-order finite difference approximation of the steady-state limit of Eq. (1), except for the last term inside the parenthesis, which is an artefact due to the discretization of the spatially varying source [53,65]. This source term artefact can be represented as the three-point stencil: $\{1 + \frac{3 - 8\Lambda}{12}, 1 - 2 \times \frac{3 - 8\Lambda}{12}, 1 + \frac{3 - 8\Lambda}{12}\}$.

In practice, the source term discretization artefact impacts the LBM accuracy towards the intended macroscopic equation by altering the effective diffusion coefficient as follows: $\mathcal{D} \to \mathcal{D}(1 + \delta)$. Consequently, the steady solution of the LBM-TRT equation becomes the solution of

following modified difference equation:

$$\mathcal{D}(1 + \delta)\,\bar{\Delta}_x^2 \phi_j - \kappa\,\phi_j + \mathcal{M} = 0, \qquad \delta := \left(\frac{8\,\Lambda - 3}{12}\right)\mathrm{Da}_g,$$
$$\mathrm{Da}_g := \frac{\kappa\,\Delta x^2}{\mathcal{D}}, \tag{24}$$

where the parameter Da_g corresponds to the grid Damköhler number, whose relation to the physical Damköhler number, Da, is given by $\mathrm{Da}_g \propto \mathrm{Da}/N_x^2$, where N_x quantifies the mesh resolution. Ideally, the source discretization artefact δ should be zero. However, as shown in Eq. (24), δ depends on three factors: (i) the physical regime, set by Da; (ii) the inverse of the mesh resolution squared, set by $1/N_x^2$; and (iii) the collision relaxation parameter, set by Λ. In order to vanish δ one of the three conditions must be satisfied: (i) Da $= 0$, which is inappropriate as it may be incompatible with the problem physics, (ii) $N_x \to \infty$, which is unfeasible as it requires operating on infinitely fine meshes, or (iii) $\Lambda = 3/8$, which among the three options is the most viable choice.

However, although fixating $\Lambda = 3/8$ cures the above mentioned source term defect in bulk [53], this choice may compromise the LBM performance with respect to other traits. For instance, it is known that $\Lambda = 1/4$ provides optimal stability [72] or $\Lambda = 3/16$ optimal boundary accuracy for some low-order reflection schemes [20,65]. That explains why users tend to operate LBM in the range $\Lambda < 3/8$, despite the simulation falling into $\delta < 0$. Worse, when $\delta < -1$, the effective diffusion coefficient becomes negative, which is expected to adversely corrupt the quality and the accuracy of the LBM steady solution; these defects will be illustrated in Section 3.2.3.

The recognition of this source discretization artefact, which is only identifiable in its full extent through an exact discrete level analysis, has motivated the development of several distinct force-based strategies to eliminate or mitigate its impact, without enforcing any restriction on the Λ choice, e.g. the works [20,65]. Among them, the improved force (IF) scheme is perhaps the simplest, though most effective, strategy. Since it was originally developed for the Brinkman-force based porous media flow models [65], the purpose of the next section is to adapt the IF scheme idea to the LBM modelling of steady reaction–diffusion systems. The IF scheme will be revisited again in Section 5.2, this time focusing on time-dependent settings.

3.2.2. Improved source scheme

The key idea of the improved force (IF) scheme [65] lies in the adoption of redefined collision rates $s_\star^-$ and $s_\star^+$ to operate in the LBM-TRT scheme, Eq. (2). The reason to have, at least, two independent collision rates will be shown below; this requirement makes the LBM-BGK model unable to handle the IF scheme. The redefined collision rates $s_\star^-$ and $s_\star^+$, or more conveniently $\Lambda_\star^- = \left(\frac{1}{s_\star^-} - \frac{1}{2}\right)$, $\Lambda_\star^+ = \left(\frac{1}{s_\star^+} - \frac{1}{2}\right)$ and $\Lambda_\star = \Lambda_\star^+ \Lambda_\star^-$ are determined through the following idea. We start by writing Eq. (21) with the re-defined collision rates, $\Lambda_\star^\pm$ and $\Lambda_\star$, so that:

$$(1 - \omega_0)\Lambda_\star^-\frac{\Delta x^2}{\Delta t}\frac{\phi_{j-1} - 2\,\phi_j + \phi_{j+1}}{\Delta x^2} - \kappa\,\phi_j + \mathcal{M}$$
$$+ \left(\omega_0\,\Lambda_\star - \frac{1}{4}\right)\Delta x^2\,\kappa\,\frac{\phi_{j-1} - 2\,\phi_j + \phi_{j+1}}{\Delta x^2} = 0. \tag{25}$$

Then, we seek to establish a relationship between these redefined collision rates $\Lambda_\star^\pm$ and the original ones $\Lambda^\pm$. This is found through the requisite that the overall coefficients pre-multiplying the Laplacian terms in Eq. (25) have to collectively match the physical diffusive coefficient $\mathcal{D} = (1 - \omega_0)\Lambda^-\frac{\Delta x^2}{\Delta t}$, Eq. (9), that is:

$$\mathcal{D} = (1 - \omega_0)\Lambda_\star^-\frac{\Delta x^2}{\Delta t} + \left[(1 - \omega_0)\,\omega_0\,\frac{\Lambda_\star^-\Lambda}{\mathcal{D}}\frac{\Delta x^2}{\Delta t} - \frac{1}{4}\right]\Delta x^2\,\kappa. \tag{26}$$

By solving Eq. (26) for $\Lambda_\star^-$, under the assumption that $\Lambda^+ = \Lambda_\star^+ = (1 - \omega_0)\frac{\Lambda}{\mathcal{D}}\frac{\Delta x^2}{\Delta t}$, one obtains:

$$\Lambda_\star^- = \frac{(4\mathcal{D} + \Delta x^2\,\kappa)}{4\,(1 - \omega_0)(\mathcal{D} + \omega_0\,\Lambda\,\Delta x^2\,\kappa)}\frac{\Delta t}{\Delta x^2}\mathcal{D}$$
$$= \frac{(4 + \mathrm{Da}_g)}{4\,(1 - \omega_0)(1 + \omega_0\,\Lambda\,\mathrm{Da}_g)}\frac{\Delta t}{\Delta x^2}\mathcal{D}, \tag{27}$$

where $\mathrm{Da}_g := \kappa\,\Delta x^2/D$. In practice, the anti-symmetric relaxation $\Lambda_\star^-$ locally adapts its value according to the physical regime parameter dictated by $\mathrm{Da} \propto \mathrm{Da}_g\, N_x^2$ [2]. Based on Eq. (27), with $D = (1-\omega_0)\Lambda^-\frac{\Delta x^2}{\Delta t}$ and $\Lambda^+ = \Lambda_\star^+$, it is straightforward deriving $\Lambda_\star$, which is given by:

$$\Lambda_\star = \frac{(4D + \Delta x^2\,\kappa)}{4\,(D + \omega_0\,\Lambda\,\Delta x^2\,\kappa)}\,\Lambda$$

$$= \frac{(4 + \mathrm{Da}_g)}{4\,(1 + \omega_0\,\Lambda\,\mathrm{Da}_g)}\,\Lambda. \tag{28}$$

The LBM-TRT running with $\Lambda_\star^-$ given by Eq. (27) and $\Lambda_\star$ given by Eq. (28) recovers an artefact-free difference approximation of the steady reaction–diffusion equation, which reads:

$$D\bar{\Delta}_x^2\phi_j - \kappa\,\phi_j + \mathcal{M} = 0, \tag{29}$$

and is valid $\forall\,\Lambda$. Although this IF scheme has been derived for a unidirectional setting, numerical evidence has shown that its main characteristics hold in more complex transport problems [20,76].

Concerning the possible numerical stability impact caused by the shifting of the original relaxation rates $\{s^+,\,s^-\}$ to the redefined ones $\{s_\star^+,\,s_\star^-\}$, this issue will be discussed in Section 4, although we anticipate that, for any Da number, the LBM-TRT is unconditionally stable with both SF and IF schemes.

3.2.3. Numerical results of the steady-state limit

This section presents numerical results that illustrate: (i) the negative effect played by the source artefact δ on the discrete solution and (ii) the visible accuracy improvements offered by the IF scheme. For the purpose of the numerical study, let us re-introduce the grid coordinate system used in Section 3.1, $x_j = j\,\Delta x$, where the index j denotes the grid numbering and $N_x + 1$ the total number of grid nodes. The spatial discretization locates the grid nodes x_j at the edges of computational cells. For a one-dimensional physical domain of size 2ℓ the size of the computational domain is $N_x\,\Delta x$, so that the individual cell size (i.e. the grid spacing parameter) is determined by $\Delta x = \frac{2\ell}{N_x}$. Note, the size of the computational cell in LBM is typically defined as $\Delta x = 1$ (simulation units).

Bulk Formulation. Consider the LBM-TRT discrete representation of the steady-state limit of Eq. (1) given by Eq. (24). The general steady-state solution to Eq. (24) reads:

$$\phi_j = \frac{\mathcal{M}}{\kappa} + A_1\,\mathcal{R}^{-x_j/\Delta x} + A_2\,\mathcal{R}^{x_j/\Delta x}, \tag{30}$$

with

$$\mathcal{R} = \frac{1}{2}\left(2 + \xi + \sqrt{\xi\,(4+\xi)}\right), \qquad \xi := \frac{\mathrm{Da}_g}{1+\delta}, \tag{31}$$

where $\mathrm{Da}_g := \frac{\kappa\,\Delta x^2}{D}$ and $\delta := \left(\frac{8\Lambda-3}{12}\right)\mathrm{Da}_g$, as originally defined in Eq. (24).

Boundary Formulation. The unknown constants $\{A_1,\,A_2\}$ in Eq. (30) are determined by the boundary conditions (BCs):

$$\phi(x = \pm\ell) = \phi_0. \tag{32}$$

The LBM prescription of the BCs, set by Eq. (32), recurs to the local second order boundary (LSOB) scheme [77], which was recently revived for fluid flow [78] and advection–diffusion [79] models. The LSOB enforces the macroscopic BCs by explicitly reconstructing the unknown incoming boundary populations based on the following TRT decomposition:

$$f_{\bar{q}}(x_b, t_n + \Delta t) = \left[e_q^+ - e_q^- + n_q^+ - n_q^- + \Delta t\left(1 - \frac{s^+}{2}\right)M_q^+\right.$$
$$\left. - \Delta t\left(1 - \frac{s^-}{2}\right)M_q^-\right]_{(x_b,t_n)}, \tag{33}$$

where $\mathbf{c}_{\bar{q}} = -\mathbf{c}_q$, $n_q^\pm = f_q^\pm - e_q^\pm$, and the boundary nodes locate at $x_b = 0$ and $x_b = N_x\,\Delta x$. The transcription of Eq. (33) into our problem gets the

following content:

$$f_{\bar{q}}(x_b, t_n + \Delta t) = \left[\omega_q\,\phi_0 + n_q^+ - n_q^- + \Delta t\left(1 - \frac{s^+}{2}\right)\omega_q\left(-\kappa\,\phi_0 + \mathcal{M}\right)\right]_{(x_b,t_n)}. \tag{34}$$

The use of Eq. (34) is local and explicit, given that $n_q^\pm$ are always available, and most importantly Eq. (34) permits exactly assigning Eq. (32) on the boundary nodes x_b, similarly to what is done by standard macroscopic (vertex-centred) difference schemes.

Discrete Solution. The substitution of Eq. (32) into Eq. (30) leads to the following exact discrete solution:

$$\phi_j = \frac{\mathcal{M}}{\kappa} + \left(\phi_0 - \frac{\mathcal{M}}{\kappa}\right)\frac{\mathcal{R}^{x_j/\Delta x} + \mathcal{R}^{N_x - x_j/\Delta x}}{1 + \mathcal{R}^{N_x}}, \tag{35}$$

with $\mathcal{R}$ given by Eq. (31).

Continuous Solution. The steady-state continuous problem formulates as the steady-state limit of Eq. (1), given by:

$$D\frac{\partial^2\phi}{\partial x^2} - \kappa\,\phi + \mathcal{M} = 0. \tag{36}$$

Eq. (36) subject to the BCs given by Eq. (32) yields the following continuous analytical solution:

$$\phi(x^\star) = \frac{\mathcal{M}}{\kappa} + \left(\phi_0 - \frac{\mathcal{M}}{\kappa}\right)\frac{\cosh\left(x^\star\sqrt{\mathrm{Da}}\right)}{\cosh\left(\sqrt{\mathrm{Da}}\right)}, \tag{37}$$

where $x^\star := x/\ell$ and $\mathrm{Da} := \frac{\kappa\ell^2}{D}$ is the Damköhler number, the physical dimensionless group governing this problem.

With discrete and continuous solutions formulated, let us now focus on their comparison. The numerical solutions are tested considering the following parameters: $\mathcal{M} = 0.01$, $\phi_0 = 0.01$, $\Delta x = 1$, $N_x = 10$, hence $\ell = N_x\,\Delta x/2 = 5$, and $\Lambda = \left\{\frac{1}{32}, \frac{1}{8}, \frac{3}{8}, \frac{1}{2}\right\}$. Fig. 2 plots the obtained numerical solutions along the three physical regimes $\mathrm{Da} = \{5, 25, 50\}$. Table 1 quantifies the associated numerical results. The numerical accuracy is defined as:

$$|L_2(\phi)| = \sqrt{\sum_j\left(\phi_j - \phi_j^{(\mathrm{analy})}\right)^2 \Big/ \sum_j(\phi_j^{(\mathrm{analy})})^2} \tag{38}$$

where sums are taken over the full computational domain.

Fig. 2 illustrates that the importance of Λ increases with the Da regime, owing to the dominance of the δ artefact with larger Da values. When $\delta < -1$ the quality of the steady solution deteriorates even further, as it becomes oscillatory due to the effective diffusion coefficient becoming negative. Although the effective diffusion coefficient is negative it is surprising that the numerical scheme still manages to converge to a unique and stable steady solution; the stability analysis presented in Section 4 will explain this result. Finally, it is important to highlight the choice $\Lambda = 3/8$, which suppresses the δ artefacts, and consequently produces an optimal accuracy over the full range of Da regimes, as quantified in Table 1. Given that, for the considered setup, the IF scheme, regardless its Λ value, is exactly equivalent to the SF scheme with $\Lambda = 3/8$, these tests provide a convincing proof on the usefulness of the IF scheme for steady-state reaction–diffusion problems. Section 5 will explore the IF scheme idea to time-dependent ones.

4. Stability analysis

4.1. Introduction

This section aims to prove that the four-level explicit finite difference scheme with a source, given by Eq. (18) with coefficients Eq. (19), is unconditionally stable for any Da number, providing $0 < \omega_0 < 1$, $0 < s^\pm < 2$ and $\kappa \geq 0$. An important outcome of this study is that, regardless the steady-state effective diffusion coefficient value, dictated by ω_0,
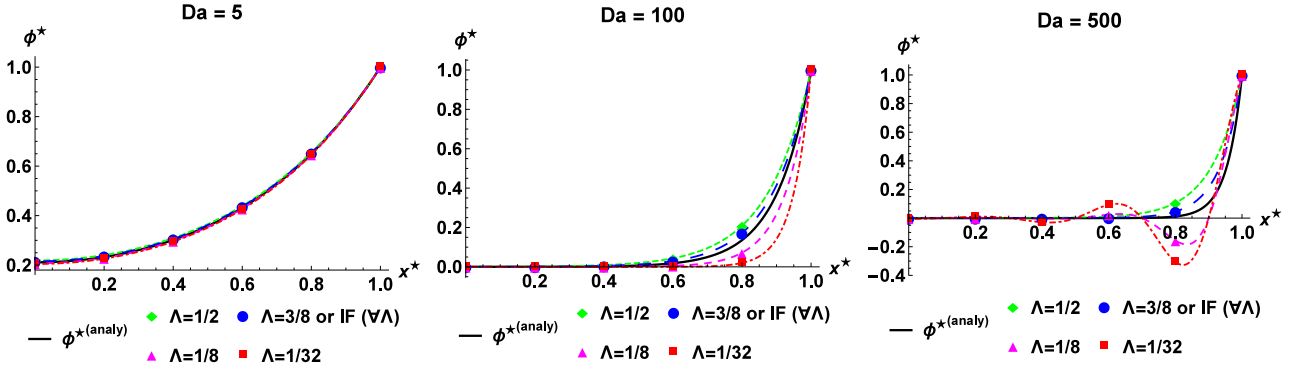
Fig. 2. LBM-TRT steady-state solutions $\phi^\star := \left(\phi - \frac{\mathcal{M}}{\kappa} \right) / \left(\phi_0 - \frac{\mathcal{M}}{\kappa} \right)$ plotted in the half-domain $x^\star = [0, 1]$, using $\mathcal{M} = 0.01$, $\phi_0 = 0.01$, $N_x = 10$ with $\Delta x = 1$ so that $\ell = 5$, and $\Lambda = \left\{ \frac{1}{32}, \frac{1}{8}, \frac{3}{8}, \frac{1}{2} \right\}$ considering the physical regimes Da = {5, 100, 500}. Steady-state analytical solution $\phi^{(analy)}$, given by Eq. (37), is represented by the black continuous line.

Table 1
Quantification of discretization parameter δ [Eq. (24)] and numerical accuracy $|L_2(\phi)|$ [Eq. (38)] for the cases shown in Fig. 2.

	Da = 5		Da = 100		Da = 500	
	δ	$|L_2(\phi)|$	δ	$|L_2(\phi)|$	δ	$|L_2(\phi)|$
$\Lambda = \frac{1}{2}$	$\frac{1}{60}$	0.0110744	$\frac{1}{3}$	0.0379866	$\frac{5}{3}$	0.0452285
$\Lambda = \frac{3}{8}$	0	0.00554203	0	0.0185286	0	0.0161546
$\Lambda = \frac{1}{8}$	$-\frac{1}{30}$	0.00572059	$-\frac{2}{3}$	0.0316577	$-\frac{10}{3}$	0.0799065
$\Lambda = \frac{1}{32}$	$-\frac{11}{240}$	0.0100138	$-\frac{11}{12}$	0.0569238	$-\frac{55}{12}$	0.156664

$s^\pm$ and κ, the LBM-TRT numerical solution will converge towards an unique solution without any restriction between Δt and Δx steps, which extends the unconditional stability condition already demonstrated for the time-dependent pure diffusion case [72,73,75], and also explains the steady-state results shown in Section 3.2.3 and in previous works [20,53,65].

The stability analysis developed in this section follows the linear von Neumann analysis that provides necessary and sufficient stability limits for periodic solutions of the evolution equation, and necessary conditions for other types of initial–boundary-value problems [80], as wall bounded solutions. While the stability of difference initial- and boundary-value problems can be studied theoretically by a number of methods, such as the method of energy inequalities [81] and the method based on the GKS-theory [82], this kind of theoretical study is beyond the scope of this work. In Section 6, this task will be verified through numerical tests. Without loss of generality, let us neglect the constant source $\mathcal{M}$ (for studies where this parameter is considered see [83–85]) and replace ϕ_j^n in Eq. (11) by the distribution function f_j^n through Eq. (8), and then take the discrete Fourier transform of $f_{q,j}^n$ in Eq. (11), which results in the following matrix equation:

$$\widehat{U}_j^{n+1} = \mathbf{G}(\theta, \omega_0, s^-, s^+, \kappa)\, \widehat{U}_j^n \tag{39}$$

where $\widehat{U}_j^n$ is the discrete Fourier transform of $f_{q,j}^n$ ($q = -1, 0, 1$) and $\mathbf{G}$ is the amplification matrix of the scheme, given by

$$\mathbf{G} = \begin{bmatrix} \left(1 - \frac{s^-}{2} - \mathcal{G}_1\right) \exp^{i\theta} & \left(\frac{s^+}{2} - \mathcal{G}_1\right) \exp^{i\theta} & \left(\frac{s^-}{2} - \mathcal{G}_1\right) \exp^{i\theta} \\ \mathcal{G}_0 & \mathcal{G}_0 - s^+ + 1 & \mathcal{G}_0 \\ \left(\frac{s^-}{2} - \mathcal{G}_{-1}\right) \exp^{-i\theta} & \left(\frac{s^+}{2} - \mathcal{G}_{-1}\right) \exp^{-i\theta} & \left(1 - \frac{s^-}{2} - \mathcal{G}_{-1}\right) \exp^{-i\theta} \end{bmatrix} \tag{40}$$

where $-\pi \leq \theta \leq \pi$ and

$$\mathcal{G}_1 = \mathcal{G}_{-1} = \frac{2}{2 + \kappa \Delta t} \left(\frac{\omega_0 s^+}{2} + \kappa \Delta t \left(\frac{1 - \omega_0}{2} + \frac{\omega_0 s^+}{4} \right) \right),$$

$$\mathcal{G}_0 = \frac{2}{2 + \kappa \Delta t} \left(\omega_0 s^+ - \kappa \Delta t\, \omega_0 \left(1 - \frac{s^+}{2} \right) \right).$$

It should be noted that, alternatively to the process that derived Eq. (40), we can directly take the Fourier transform of the multi-level finite difference scheme described by Eq. (18), with coefficients represented by Eq. (19), so that the alternative transformation $\widehat{U}_j^{n+1} = \mathbf{H}\, \widehat{U}_j^n$ takes the following amplification matrix:

$$\mathbf{H} = \begin{bmatrix} 2\alpha_1 \cos\theta + \alpha_2 & 2\beta_1 \cos\theta + \beta_2 & \gamma \\ 1 & 0 & 0 \\ 0 & 1 & 0 \end{bmatrix}$$

Both amplification matrices, $\mathbf{G}$ and $\mathbf{H}$, lead to the same characteristic polynomial, given by:

$$p(z) = \lambda^3 + p_2 \lambda^2 + p_1 \lambda + p_0 \tag{41}$$

with coefficients

$$p_0 = -\frac{2}{2 + \kappa \Delta t} \left[(s^- - 1)(s^+ - 1) - \kappa \Delta t (s^- - 1)(s^+ - 1) \right], \tag{42}$$

$$\begin{aligned} p_1 = &-\frac{2}{2 + \kappa \Delta t} \left[2 \left(\frac{\omega_0 s^- s^+}{2} - \frac{\omega_0 s^+}{2} - \frac{s^- s^+}{2} + s^+ + \frac{s^-}{2} - 1 \right) \cos\theta \right. \\ &- 2\kappa \Delta t \left(-\frac{\omega_0 s^- s^+}{4} + \frac{\omega_0 s^+}{4} + \frac{\omega_0 s^-}{2} + \frac{s^+ s^-}{4} - \frac{s^-}{4} - \frac{\omega_0}{2} \right) \cos\theta \\ &+ \left(-\omega_0 s^- s^+ + \omega_0 s^+ + s^- - 1 \right) \\ &\left. - \kappa \Delta t \left(\frac{\omega_0 s^- s^+}{2} - \frac{\omega_0 s^+}{2} - \omega_0 s^- + \frac{s^-}{2} + \omega_0 - \frac{1}{2} \right) \right], \end{aligned} \tag{43}$$

$$\begin{aligned} p_2 = &-\frac{2}{2 + \kappa \Delta t} \left[2 \left(1 - \frac{s^-}{2} - \frac{\omega_0 s^+}{2} \right) \cos\theta - 2\kappa \Delta t \left(\frac{\omega_0 s^+}{4} + \frac{s^-}{4} - \frac{\omega_0}{2} \right) \cos\theta \right. \\ &\left. + \left(\omega_0 s^+ - s^+ + 1 \right) - \kappa \Delta t \left(-\frac{\omega_0 s^+}{2} + \frac{s^+}{2} + \omega_0 - \frac{1}{2} \right) \right]. \end{aligned} \tag{44}$$

Next, we will show that the roots of the characteristic polynomial $p(\lambda)$ expressed by λ_k ($k = 1, 2$, and 3) satisfy the condition $|\lambda_k| \leq 1$.

4.2. Routh–Hurwitz stability criterion

For the sake of the stability study, we follow [75] and introduce the following linear fractional transformation:

$$\lambda = \frac{1 + z}{1 - z}, \qquad z \in \mathbb{C}, \tag{45}$$

where the unit circle $|\lambda| = 1$ and the field $|\lambda| < 1$ are mapped to the imaginary axis [Re(z) = 0] and left-half plane [Im(z) < 0]. Here, $\mathbb{C}$, Re and Im express the complex-number field, the real and the imaginary parts of a complex number, respectively. Introducing the

transformation, given by Eq. (45), into $p(z) = \lambda^3 + p_2 \lambda^2 + p_1 \lambda + p_0$, Eq. (41), we obtain:

$$
\begin{aligned}
(1-z)^3 p\left(\frac{1+z}{1-z}\right) &= (1+z)^3 + p_2(1-z)(1+z)^2 + p_1(1-z)^2(1+z) \\
&\quad + p_0(1-z)^3 \\
&= \underbrace{(1 - p_0 + p_1 - p_2)}_{a_0} z^3 + \underbrace{(3 + 3p_0 - p_1 - p_2)}_{a_1} z^2 \\
&\quad + \underbrace{(3 - 3p_0 - p_1 + p_2)}_{a_2} z + \underbrace{(1 + p_0 + p_1 + p_2)}_{a_3}.
\end{aligned}
\tag{46}
$$

According to the Routh–Hurwitz stability criterion [86], the roots of the characteristic polynomial $p(\lambda)$ are located in the field $|\lambda| < 1$ providing the following conditions are satisfied:

$$a_0 = 1 - p_0 + p_1 - p_2 > 0, \tag{47a}$$

$$a_1 = 3 + 3p_0 - p_1 - p_2 > 0, \tag{47b}$$

$$a_2 = 3 - 3p_0 - p_1 + p_2 > 0, \tag{47c}$$

$$a_3 = 1 + p_0 + p_1 + p_2 > 0, \tag{47d}$$

$$a_1 a_2 - a_0 a_3 = 1 - p_1 + p_0 p_2 - p_0^2 > 0. \tag{47e}$$

By taking the sums of Eqs. (47a) and (47c), and Eqs. (47b) and (47d), we can equivalently rewrite Eq. (47) as [75]

$$1 - p_0 + p_1 - p_2 > 0, \tag{48a}$$

$$1 - p_0 > 0, \tag{48b}$$

$$1 + p_0 > 0, \tag{48c}$$

$$1 + p_0 + p_1 + p_2 > 0, \tag{48d}$$

$$1 - p_1 + p_0 p_2 - p_0^2 > 0. \tag{48e}$$

Invoking the following conditions: $\cos\theta \neq 1$, $\kappa \geq 0$, and $0 < \omega_0 < 1$ together with $0 < s^\pm < 2$, let us now prove the five inequalities stated above.

1. Eq. (48a) is proven as:

$$
\begin{aligned}
&1 - p_0 + p_1 - p_2 \\
&= \frac{2}{2 + \kappa \Delta t}\left[\underbrace{\left((2 - s^-)(2 - s^+)(1 + \cos\theta) + \omega_0 s^- s^+(1 - \cos\theta)\right)}_{>0} \right. \\
&\quad \left. + \kappa \frac{\Delta t}{2} \underbrace{\left((1 - w_0)s^-(2 - s^+)(1 + \cos\theta)\right)}_{>0} \right] > 0
\end{aligned}
\tag{49}
$$

2. Eq. (48b) is proven as:

$$
\begin{aligned}
1 - p_0 &= \frac{2}{2 + \kappa \Delta t}\left[\underbrace{\left(1 + (1 - s^-)(1 - s^+)\right)}_{>0} \right. \\
&\quad \left. + \kappa \frac{\Delta t}{2} \underbrace{\left(1 - (1 - s^-)(1 - s^+)\right)}_{>0} \right] > 0
\end{aligned}
\tag{50}
$$

3. Eq. (48c) is proven as:

$$
\begin{aligned}
1 + p_0 &= \frac{2}{2 + \kappa \Delta t}\left[\underbrace{\left(1 - (1 - s^-)(1 - s^+)\right)}_{>0} \right. \\
&\quad \left. + \kappa \frac{\Delta t}{2} \underbrace{\left(1 + (1 - s^-)(1 - s^+)\right)}_{>0} \right] > 0
\end{aligned}
\tag{51}
$$

4. Eq. (48d) is proven as:

$$
\begin{aligned}
1 + p_0 + p_1 + p_2 &= \frac{2}{2 + \kappa \Delta t}\left[\underbrace{\left((1 - w_0)(2 - s^-)s^+(1 - \cos\theta)\right)}_{>0} \right. \\
&\quad \left. + \kappa \frac{\Delta t}{2} \underbrace{\left((s^- s^+)(1 + \cos\theta) + \omega_0(2 - s^-)(2 - s^+)(1 - \cos\theta)\right)}_{>0} \right] > 0
\end{aligned}
\tag{52}
$$

5. Eq. (48e) is slightly more evolving to prove; its proof goes as follows:

$$
\begin{aligned}
1 - p_1 + p_0 p_2 - p_0^2 &= \frac{4}{(2 + \kappa \Delta t)^2}\left[\left(\mathcal{A}_1(1 - \cos\theta) + \mathcal{B}_1\right) \right. \\
&\quad + \kappa \frac{\Delta t}{2}\left(\mathcal{A}_2(1 - \cos\theta) + \mathcal{B}_2\right) \\
&\quad \left. + \kappa^2 \frac{\Delta t^2}{4}\left(\mathcal{A}_3(1 - \cos\theta) + \mathcal{B}_3\right) \right],
\end{aligned}
\tag{53}
$$

with coefficients

$$\mathcal{A}_1 = s^-(2 - s^-)(1 - s^+) + \omega_0 s^+(1 - s^-)(2 - s^+) \tag{54a}$$

$$\mathcal{B}_1 = s^- s^+\left(1 - (1 - s^-)(1 - s^+)\right) \tag{54b}$$

$$\mathcal{A}_2 = 4(1 - \omega_0)(1 - s^-)(1 - s^+) \tag{54c}$$

$$\mathcal{B}_2 = 2\left(1 - (1 - s^-)(1 - s^+)\right)^2 \tag{54d}$$

$$\mathcal{A}_3 = -\left(s^-(2 - s^-)(1 - s^+) + \omega_0 s^+(1 - s^-)(2 - s^+)\right) \tag{54e}$$

$$\mathcal{B}_3 = (2 - s^-)(2 - s^+)\left(1 - (1 - s^-)(1 - s^+)\right) \tag{54f}$$

Now, let us look at Eq. (53) under the following conditions:

(i) If $0 < s^- \leq 1$ and $0 < s^+ \leq 1$ then:

$$\mathcal{A}_1 = \underbrace{s^-(2 - s^-)(1 - s^+)}_{\geq 0} + \underbrace{\omega_0 s^+(1 - s^-)(2 - s^+)}_{\geq 0} \geq 0$$

$$\mathcal{B}_1 = s^- s^+\left(1 - (1 - s^-)(1 - s^+)\right) > 0$$

$$\mathcal{A}_1(1 - \cos\theta) + \mathcal{B}_1 > 0$$

$$
\begin{aligned}
\mathcal{A}_2(1 - \cos\theta) + \mathcal{B}_2 &= \underbrace{4(1 - \omega_0)(1 - s^-)(1 - s^+)(1 - \cos\theta)}_{\geq 0} \\
&\quad + 2\underbrace{\left(1 - (1 - s^-)(1 - s^+)\right)^2}_{>0} > 0
\end{aligned}
$$

$$
\begin{aligned}
\mathcal{A}_3(1 - \cos\theta) + \mathcal{B}_3 &> -2\left(s^-(2 - s^-)(1 - s^+)\right. \\
&\quad \left. + s^+(1 - s^-)(2 - s^+)\right) + \mathcal{B}_3
\end{aligned}
$$

$$= s^- s^+ \underbrace{\left(1 - (1 - s^-)(1 - s^+)\right)}_{>0} > 0$$

(ii) If $0 < s^- \leq 1$ and $1 < s^+ < 2$ then:

$$\mathcal{A}_1 = s^-(2 - s^-)(1 - s^+) + \underbrace{\omega_0 \, s^+(1 - s^-)(2 - s^+)}_{\geq 0}$$

$$\geq s^-(2 - s^-)(1 - s^+)$$

$$\mathcal{A}_1(1 - \cos\theta) + \mathcal{B}_1 \geq 2\,s^-(2 - s^-)(1 - s^+) + \mathcal{B}_1$$

$$= \underbrace{s^-(2 - s^+)\left(1 + (1 - s^-)(1 - s^+)\right)}_{>0} > 0$$

$$\mathcal{A}_2(1 - \cos\theta) + \mathcal{B}_2 > 8(1 - s^-)(1 - s^+) + \mathcal{B}_2$$

$$= 2\underbrace{\left(1 + (1 - s^-)(1 - s^+)\right)^2}_{>0} > 0$$

$$\mathcal{A}_3(1 - \cos\theta) + \mathcal{B}_3 > -2\left(s^+(1 - s^-)(2 - s^+)\right) + \mathcal{B}_3$$

$$= \underbrace{s^-(2 - s^+)\left(1 + (1 - s^-)(1 - s^+)\right)}_{>0} > 0$$

(iii) If $1 < s^- < 2$ and $0 < s^+ \leq 1$ then:

$$\mathcal{A}_1 = \underbrace{s^-(2 - s^-)(1 - s^+)}_{>0} + \omega_0 \, s^+(1 - s^-)(2 - s^+)$$

$$\geq \omega_0 \, s^+(1 - s^-)(2 - s^+) > s^+(1 - s^-)(2 - s^+)$$

$$\mathcal{A}_1(1 - \cos\theta) + \mathcal{B}_1 > s^+(1 - s^-)(2 - s^+) + \mathcal{B}_1$$

$$= \underbrace{s^+(2 - s^-)\left(1 + (1 - s^-)(1 - s^+)\right)}_{>0} > 0$$

$$\mathcal{A}_2(1 - \cos\theta) + \mathcal{B}_2 > 8(1 - s^-)(1 - s^+) + \mathcal{B}_2$$

$$= 2\underbrace{\left(1 + (1 - s^-)(1 - s^+)\right)^2}_{>0} > 0$$

$$\mathcal{A}_3(1 - \cos\theta) + \mathcal{B}_3 > -2\left(s^-(2 - s^-)(1 - s^+)\right) + \mathcal{B}_3$$

$$= \underbrace{s^+(2 - s^-)\left(1 + (1 - s^-)(1 - s^+)\right)}_{>0} > 0$$

(iv) If $1 < s^- < 2$ and $1 < s^+ < 2$ then:

$$\mathcal{A}_1 = s^-(2 - s^-)(1 - s^+) + \omega_0 \, s^+(1 - s^-)(2 - s^+)$$

$$> \underbrace{s^-(2 - s^-)(1 - s^+) + s^+(1 - s^-)(2 - s^+)}_{= C_1}$$

$$\mathcal{A}_1(1 - \cos\theta) + \mathcal{B}_1 > 2\,\mathcal{A}_1 + \mathcal{B}_1 > 2\,C_1 + \mathcal{B}_1$$

$$= \underbrace{(2 - s^-)(2 - s^+)\left(1 + (1 - s^-)(1 - s^+)\right)}_{>0} > 0$$

$$\mathcal{A}_2(1 - \cos\theta) + \mathcal{B}_2 = \underbrace{4(1 - \omega_0)(1 - s^-)(1 - s^+)(1 - \cos\theta)}_{\geq 0}$$

$$+ 2\underbrace{\left(1 - (1 - s^-)(1 - s^+)\right)^2}_{>0} > 0$$

$$\mathcal{A}_3(1 - \cos\theta) + \mathcal{B}_3 > -2\left(s^-(2 - s^-)(1 - s^+)\right)$$

$$+ s^+(1 - s^-)(2 - s^+)\Big) + \mathcal{B}_3$$

$$= s^- s^+ \underbrace{\left(1 - (1 - s^-)(1 - s^+)\right)}_{>0} > 0$$

The ensemble of results (i)-(iv) proves Eq. (48e).

Overall, the proofs presented in Eqs. (48a), (48b), (48c), (48d) and (48e) establish that the roots of Eq. (46), or equivalently of Eq. (41), are located in the field $|\lambda| < 1$ under the condition of $\cos\theta \neq 1$.

As for the remaining condition, $\cos\theta = 1$, it can be established in many ways. For example, the reductive approach [87] may be followed, as proposed in the work [75] or, perhaps even simpler, one may treat this singular case, $\cos\theta = 1$, by realizing that the roots of the characteristic polynomial $p(\lambda)$ are continuous functions of $\cos\theta$ and, therefore, they must satisfy the condition $|\lambda_k| < 1$ for $k = 1, 2$, and 3 also in this case.

From the above exposed, this analysis proves that the roots of the characteristic polynomial, as defined in Eq. (46), satisfy the condition $|\lambda_k| < 1$ for $k = 1, 2$, and 3, implying that the LBM-TRT scheme, Eq. (2), with a source, $\kappa \geq 0$, is *unconditionally stable* for $0 < \omega_0 < 1$ and $0 < s^\pm < 2$. This is a valuable asset of the LBM-TRT scheme as, generally, explicit numerical schemes tend to be conditionally stable only.

5. Accuracy analysis

This section undertakes an accuracy analysis of the four-level finite difference scheme derived in Eq. (17). The goal of this analysis is twofold: (i) to reveal the structure of the leading order truncation errors of the LBM-TRT scheme with a source, Section 5.1, and (ii) to develop strategies that are capable of improving the numerical scheme accuracy, Section 5.2.

5.1. Standard source (SF)

Consider the Taylor series of ϕ about the position $x_j = j\,\Delta x$ and time $t_n = n\,\Delta t$, defined as follows:

$$\phi(x_j + k\,\Delta x, t_n + m\,\Delta t) = \phi(x_j, t_n)$$
$$+ \sum_{r=1}^{o} \frac{1}{r!} \sum_{s=0}^{r} \binom{r}{s} (k\,\Delta x)^s (m\,\Delta t)^{s-r} \left.\frac{\partial^r \phi}{\partial x^r}\right|_{(x_j, t_n)} \quad (55)$$

where $\binom{r}{s} = \frac{r!}{(r-s)!\,s!}$ is the binomial coefficient.

Applying Eq. (55), up to fourth order ($o = 4$), over each term in Eq. (18), and then collecting the coefficients of common terms, we arrive at the following equation:

$$\left(1 + 2\beta_1 + \beta_2 + 2\gamma\right)\Delta t \left[\frac{\partial\phi}{\partial t}\right]_j^n = \left(-1 + 2\alpha_1 + \alpha_2 + 2\beta_1 + \beta_2 + \gamma\right)\phi_j^n$$

$$+ \left(\alpha_1 + \beta_1\right)\Delta x^2 \left[\frac{\partial^2\phi}{\partial x^2}\right]_j^n + \zeta\,\mathcal{M}$$

$$+ \left(\alpha_1 + \beta_1\right)\frac{\Delta x^4}{12}\left[\frac{\partial^4\phi}{\partial x^4}\right]_j^n$$

$$- \beta_1\,\Delta x^2\,\Delta t\left[\frac{\partial^3\phi}{\partial x^2\partial t}\right]_j^n$$

$$+ \left(-1 + 2\beta_1 + \beta_2 + 4\gamma\right)\frac{\Delta t^2}{2}\left[\frac{\partial^2\phi}{\partial t^2}\right]_j^n$$

$$+ \cdots$$

$$(56)$$

Explicitly, substituting the content of the coefficients, given by Eq. (20), into Eq. (56), then multiplying each term by $\left(1 + \kappa\,\frac{\Delta t}{2}\right)/(s^+ s^-)$ and

finally taking into account that $\mathcal{D} = (1 - \omega_0) \Lambda^- \frac{\Delta x^2}{\Delta t}$, it results in the following equation:

$$
\begin{aligned}
\left[\frac{\partial \phi}{\partial t}\right]_j^n =& D \left[\frac{\partial^2 \phi}{\partial x^2}\right]_j^n - \kappa\, \phi_j^n + \mathcal{M} \\
& - \kappa \left(\Lambda^+ + \Lambda^- - \frac{1}{2}\right) \Delta t \left[\frac{\partial \phi}{\partial t}\right]_j^n \\
& + \kappa \left(\Lambda - \frac{1}{4} - (1 - \omega_0)\,\Lambda\right) \Delta x^2 \left[\frac{\partial^2 \phi}{\partial x^2}\right]_j^n \\
& + \frac{1}{12} D \Delta x^2 \left[\frac{\partial^4 \phi}{\partial x^4}\right]_j^n + \underbrace{\frac{1}{12} \kappa \left(\Lambda - \frac{1}{4} - (1 - \omega_0)\,\Lambda\right) \Delta x^4 \left[\frac{\partial^4 \phi}{\partial x^4}\right]_j^n}_{\mathcal{O}(\Delta x^4)\text{ is higher order}} \\
& + \underbrace{\left(\Lambda - \frac{1}{4} - (1 - \omega_0)\left(\frac{\Lambda^-}{2} - \frac{1}{4}\right)\right) \Delta x^2 \left[\frac{\partial^3 \phi}{\partial x^2 \partial t}\right]_j^n}_{} \\
& \underbrace{- \frac{1}{2} \kappa \left(\Lambda - \frac{1}{4} - (1 - \omega_0)\left(\Lambda - \frac{\Lambda^+}{2}\right)\right) \Delta t\, \Delta x^2 \left[\frac{\partial^3 \phi}{\partial x^2 \partial t}\right]_j^n}_{\mathcal{O}(\Delta t\, \Delta x^2)\text{ is higher order}} \\
& - \left(\Lambda^+ + \Lambda^- - \frac{1}{2}\right) \Delta t \left[\frac{\partial^2 \phi}{\partial t^2}\right]_j^n \\
& \underbrace{- \kappa \left(\Lambda - \frac{\Lambda^+ + \Lambda^-}{2} + \frac{1}{2}\right) \Delta t^2 \left[\frac{\partial^2 \phi}{\partial t^2}\right]_j^n + \cdots}_{\mathcal{O}(\Delta t^2)\text{ is higher order}}
\end{aligned}
\tag{57}
$$

In the equation above, the diffusive scaling relationship $\Delta t \propto \Delta x^2$ is used to identify the higher order terms.

Now, let us invoke the target differential equation, Eq. (1), to derive the following relations:

$$
\begin{aligned}
\left[\frac{\partial \phi}{\partial t}\right]_j^n &= D \left[\frac{\partial^2 \phi}{\partial x^2}\right]_j^n - \kappa\, \phi_j^n + \mathcal{M}, \\
\left[\frac{\partial^2 \phi}{\partial t^2}\right]_j^n &= D^2 \left[\frac{\partial^4 \phi}{\partial x^4}\right]_j^n - 2\,D\,\kappa \left[\frac{\partial^2 \phi}{\partial x^2}\right]_j^n + \kappa^2\, \phi_j^n - \kappa\, \mathcal{M}, \\
\left[\frac{\partial^3 \phi}{\partial x^2 \partial t}\right]_j^n &= D \left[\frac{\partial^4 \phi}{\partial x^4}\right]_j^n - \kappa \left[\frac{\partial^2 \phi}{\partial x^2}\right]_j^n.
\end{aligned}
\tag{58}
$$

Eqs. (58) enable us to substitute the time derivative terms on the right-hand side of Eq. (57) by equivalent terms only involving spatial derivatives, which leads to:

$$
\begin{aligned}
\left[\frac{\partial \phi}{\partial t}\right]_j^n =& D \left[\frac{\partial^2 \phi}{\partial x^2}\right]_j^n - \kappa\, \phi_j^n + \mathcal{M} \\
& - \left(\Lambda^+ + \Lambda^- - \frac{1}{2}\right) \Delta t \left(D\,\kappa \left[\frac{\partial^2 \phi}{\partial x^2}\right]_j^n - \kappa^2 \cancel{\phi_j^n} + \cancel{\kappa \mathcal{M}}\right) \\
& + \left(\Lambda - \frac{1}{4} - (1 - \omega_0)\,\Lambda\right) \Delta x^2\, \kappa \left[\frac{\partial^2 \phi}{\partial x^2}\right]_j^n + \frac{1}{12} \Delta x^2\, D \left[\frac{\partial^4 \phi}{\partial x^4}\right]_j^n \\
& + \left(\Lambda - \frac{1}{4} - (1 - \omega_0)\left(\frac{\Lambda^-}{2} - \frac{1}{4}\right)\right) \\
& \times \Delta x^2 \left(D \left[\frac{\partial^4 \phi}{\partial x^4}\right]_j^n - \kappa \left[\frac{\partial^2 \phi}{\partial x^2}\right]_j^n\right) \\
& - \left(\Lambda^+ + \Lambda^- - \frac{1}{2}\right) \Delta t \left(D^2 \left[\frac{\partial^4 \phi}{\partial x^4}\right]_j^n - 2\,D\,\kappa \left[\frac{\partial^2 \phi}{\partial x^2}\right]_j^n\right. \\
& \left. + \kappa^2 \cancel{\phi_j^n} - \cancel{\kappa \mathcal{M}}\right) + \cdots
\end{aligned}
\tag{59}
$$

Finally, by grouping the coefficients of common terms, and considering $\mathcal{D} = (1 - \omega_0) \Lambda^- \frac{\Delta x^2}{\Delta t}$, we can re-write Eq. (59) in the following compact

form:

$$
\begin{aligned}
\left[\frac{\partial \phi}{\partial t}\right]_j^n =& D \left[\frac{\partial^2 \phi}{\partial x^2}\right]_j^n - \kappa\, \phi_j^n + \mathcal{M} \\
& + \left[\left(\Lambda - \frac{1}{6}\right) - (1 - \omega_0)\left(\Lambda^{-2} + \Lambda - \frac{1}{4}\right)\right] D \Delta x^2 \left[\frac{\partial^4 \phi}{\partial x^4}\right]_j^n \\
& + (1 - \omega_0)\left(\Lambda^{-2} - \frac{1}{4}\right) \kappa \Delta x^2 \left[\frac{\partial^2 \phi}{\partial x^2}\right]_j^n + \mathcal{O}(\Delta t^2, \Delta x^4).
\end{aligned}
\tag{60}
$$

It is interesting to note that the coefficient of the leading order diffusion correction in Eq. (60) matches that derived in previous works with the TRT [47], MRT [75] or BGK [73] schemes, after doing the required adjustments.

Eq. (60) indicates that, upon fixating the diffusion coefficient D (or its discrete counterpart $\epsilon = D \frac{\Delta t}{\Delta x^2}$) and the source term coefficient κ, the LBM-TRT scheme with the source term modelled via the SF scheme is first-order accurate in time and second-order accurate in space $\mathcal{O}(\Delta t, \Delta x^2)$. This is the traditional accuracy of LBM. Second-order accuracy in time and fourth-order accuracy in space $\mathcal{O}(\Delta t^2, \Delta x^4)$ can be achieved through the canceling of the second-order truncation errors in Eq. (60), a condition set by the following system of equations:

$$
\begin{cases}
\epsilon = (1 - \omega_0)\, \Lambda^-, \\
\left(\Lambda - \frac{1}{6}\right) - (1 - \omega_0)\left(\Lambda^{-2} + \Lambda - \frac{1}{4}\right) = 0, \\
(1 - \omega_0)\left(\Lambda^{-2} - \frac{1}{4}\right) = 0.
\end{cases}
\tag{61}
$$

The solution of Eq. (61) is given below and is also plotted in Fig. 3.

$$
\begin{cases}
\omega_0 = 1 - 2\,\epsilon \\
\Lambda^- = \frac{1}{2} \\
\Lambda^+ = \frac{1}{3(1 - 2\epsilon)}
\end{cases}
\implies
\begin{cases}
\omega_0 = 1 - 2\,\epsilon \\
s^- = 1 \\
s^+ = \frac{6 - 12\,\epsilon}{5 - 6\,\epsilon}
\end{cases}
\tag{62}
$$

In conclusion, giving ϵ, the improvement of the SF scheme accuracy to $\mathcal{O}(\Delta t^2, \Delta x^4)$ requires assigning the three free parameters ω_0, s^- and s^+ to the specific values dictated by Eq. (62), which sets a huge constraint on the scheme flexibility.

5.2. Improved source (IF)

In order to improve the scheme accuracy, without compromising its flexibility as happening with the SF scheme, let us adapt the IF original idea [65] and re-write the LBM-TRT algorithm assuming it runs with the re-defined relaxation parameters $\{s_\star^+, s_\star^-\}$ or equivalently $\Lambda_\star^\pm = \left(\frac{1}{s_\star^\pm} - \frac{1}{2}\right)$. By repeating the procedure summarized in Section 5.1, we arrive at:

$$
\begin{aligned}
\left[\frac{\partial \phi}{\partial t}\right]_j^n =& (1 - \omega_0)\,\Lambda_\star^- \frac{\Delta x^2}{\Delta t} \left[\frac{\partial^2 \phi}{\partial x^2}\right]_j^n - \kappa\, \phi_j^n + \mathcal{M} \\
& + \left[\left(\Lambda_\star - \frac{1}{6}\right) - (1 - \omega_0)\left(\Lambda_\star^{-2} + \Lambda_\star - \frac{1}{4}\right)\right] D \Delta x^2 \left[\frac{\partial^4 \phi}{\partial x^4}\right]_j^n \\
& + (1 - \omega_0)\left(\Lambda_\star^{-2} - \frac{1}{4}\right) \kappa \Delta x^2 \left[\frac{\partial^2 \phi}{\partial x^2}\right]_j^n + \mathcal{O}(\Delta t^2, \Delta x^4).
\end{aligned}
\tag{63}
$$

Contrary to the steady-state case presented in Section 3.2.2, the time-dependent IF procedure developed below will be focused on the second-order derivative terms, requiring their coefficients to satisfy the following condition:

$$
D = (1 - \omega_0)\, \Lambda_\star^- \frac{\Delta x^2}{\Delta t} + (1 - \omega_0)\left(\Lambda_\star^{-2} - \frac{1}{4}\right) \kappa \Delta x^2,
\tag{64}
$$

where the effective diffusion coefficient D remains determined by the original s^- relaxation rate as $D = (1 - \omega_0)\, \Lambda^- \frac{\Delta x^2}{\Delta t}$. By solving Eq. (64) for $\Lambda_\star^-$, the only meaningful solution is:

$$
\Lambda_\star^- = -\frac{1}{2\,\kappa\,\Delta t} + \sqrt{\frac{1}{4} + \frac{1}{4\,\kappa^2\,\Delta t^2} + \frac{D}{(1 - \omega_0)\,\kappa\,\Delta x^2}},
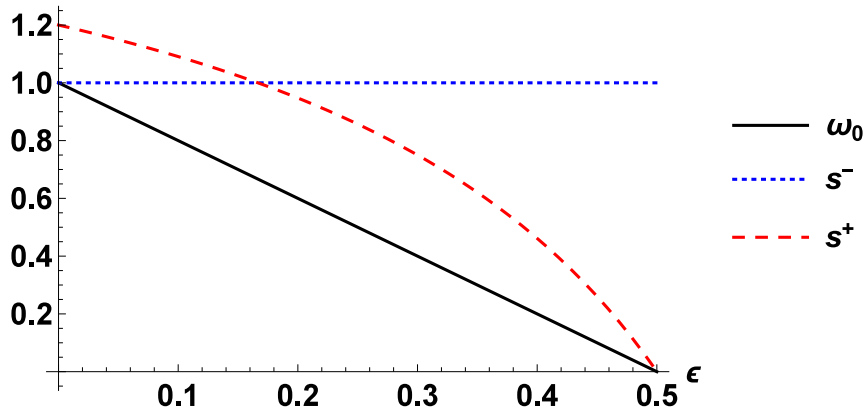\tag{65}
$$

Fig. 3. Values of ω_0, s^- and s^+ as function of ϵ, which guarantee the $\mathcal{O}(\Delta t^2, \Delta x^4)$ accuracy in the SF scheme.

and, by keeping up with the original IF model philosophy, the even relaxation parameter $\Lambda_\star^+$ remains given by:

$$\Lambda_\star^+ = \Lambda^+. \tag{66}$$

At this point, it is worth mentioning that a truncation error analysis developed to improve the scheme accuracy, similarly to what was done for the original relaxation rates in Section 5.1, becomes significantly more cumbersome as it will require solving a system of non-linear equations that is strongly dependent on κ, meaning that a new solution must be determined each time the physical regime Da and/or the grid resolution N_x varies. On this basis, the gains in numerical accuracy may not pay off the added implementation complexity and computational strain. Fortunately, a simplification is possible that does not compromise these assets, while holding the intended level of accuracy. Through a careful inspection of the order of magnitude terms in Eq. (64), it is found that original and re-defined relaxation parameters relate as:

$$\Lambda^- = \Lambda_\star^- + \mathcal{O}(\Delta x^2). \tag{67}$$

By exploring Eq. (67) it is possible to devise strategies that improve the scheme accuracy while holding the leading order diffusion correction term controlled by the original relaxations parameters $\Lambda^\pm$ (instead of the new ones $\Lambda_\star^\pm$, which are Da dependent). Thus, within the intended order of approximation, the following equation is valid:

$$\left[\frac{\partial \phi}{\partial t}\right]_j^n = \underbrace{\left((1-\omega_0)\Lambda_\star^- \frac{\Delta x^2}{\Delta t} + (1-\omega_0)\left(\Lambda_\star^{-2} - \frac{1}{4}\right)\kappa \Delta x^2\right)}_{=D}\left[\frac{\partial^2 \phi}{\partial x^2}\right]_j^n$$

$$- \kappa \phi_j^n + \mathcal{M} \tag{68}$$

$$+ \left[\left(\Lambda - \frac{1}{6}\right) - (1-\omega_0)\left(\Lambda^{-2} + \Lambda - \frac{1}{4}\right)\right] D \Delta x^2 \left[\frac{\partial^4 \phi}{\partial x^4}\right]_j^n$$

$$+ \mathcal{O}(\Delta t^2, \Delta x^4).$$

Eq. (68) indicates that the IF model reaches the $\mathcal{O}(\Delta x^4, \Delta t^2)$ accuracy under the following conditions:

$$\begin{cases} \epsilon = (1-\omega_0)\Lambda^-, \\ \left(\Lambda - \frac{1}{6}\right) - (1-\omega_0)\left(\Lambda^{-2} + \Lambda - \frac{1}{4}\right) = 0. \end{cases} \tag{69}$$

Compared to the SF model, Eq. (61), where to reach the $\mathcal{O}(\Delta t^2, \Delta x^4)$ accuracy it requires fixing all three free parameters ω_0, Λ^- and Λ^+, the IF scheme, Eq. (69), releases this constraint only requiring two conditions. Thus, it liberates one free parameter to improve other features of the numerical scheme, such as attempting the support of higher orders of accuracy [47,75] or removing possible discrete effects on the boundary conditions [39].

To conclude, it is important to demonstrate that the IF scheme preserves the unconditional stability of the SF scheme, proved in Section 4. As starting point, let us note that the IF scheme only differs from
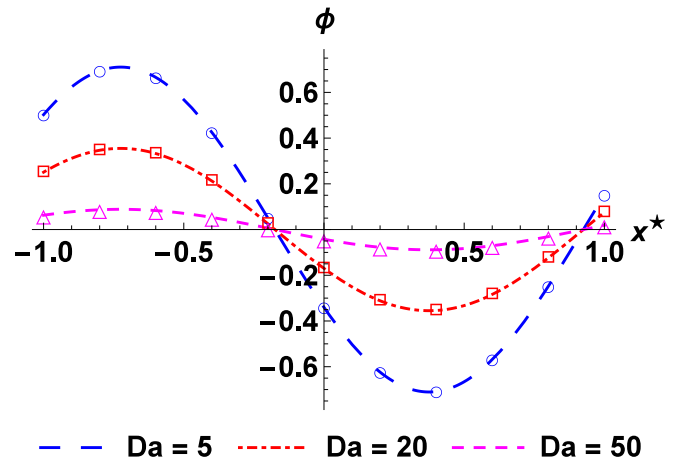

Fig. 4. Benchmark 1. Time decaying unbounded wave with $t^\star = 0.05$, $D = 0.1$, $N_x = 10$, $\Delta x = 1$, $\ell = N_x \Delta x/2 = 5$. Continuous lines depict the analytical solutions, given by Eq. (72). Markers indicate the nodal values obtained with SF scheme, using $s^- = 1$ and $s^+ = 42/41$.

the SF in the anti-symmetric relaxation mode $\Lambda_\star^-$. Hence, the stability results put forward in Section 4 hold valid providing one can prove that $\Lambda_\star^- > 0$, within the parameter space $0 < \omega_0 < 1$, $\kappa \geq 0$ and $D > 0$. Under these conditions, it is evident that $\frac{1}{4} + \frac{D}{(1-\omega_0)\kappa \Delta x^2} > 0$, which is sufficient to prove $\sqrt{\frac{1}{4} + \frac{1}{4\kappa^2 \Delta t^2} + \frac{D}{(1-\omega_0)\kappa \Delta x^2}} > \frac{1}{2\kappa \Delta t}$. Then, according to Eq. (65), it follows that the previous inequality is synonymous to $\Lambda_\star^- > 0$ for $\kappa > 0$. The limit $\kappa = 0$ recovers $\Lambda_\star^- = \Lambda^-$. These analyses establish the IF scheme as unconditionally stable.

6. Numerical tests

This section focuses on the numerical accuracy of SF and IF schemes to solve Eq. (1) under different initial and boundary conditions. Table 2 summarizes the main characteristics of the benchmark tests considered here. Their solutions will be presented in terms of the two non-dimensional governing parameters:

(1) Damköhler number: $\text{Da} = \frac{\kappa \ell^2}{D}$,

(2) Fourier number: $\text{Fo} = \frac{t D}{\ell^2} = t^\star$,

and the spatial coordinate $x \in [-\ell, \ell]$ is rescaled in non-dimensional form as $x^\star = \frac{x}{\ell} \in [-1, 1]$.

The numerical implementation is based on Eq. (18) with coefficients given by Eq. (19). Since the solver consists of a four-level difference scheme, its complete initialization requires the initial values of ϕ at
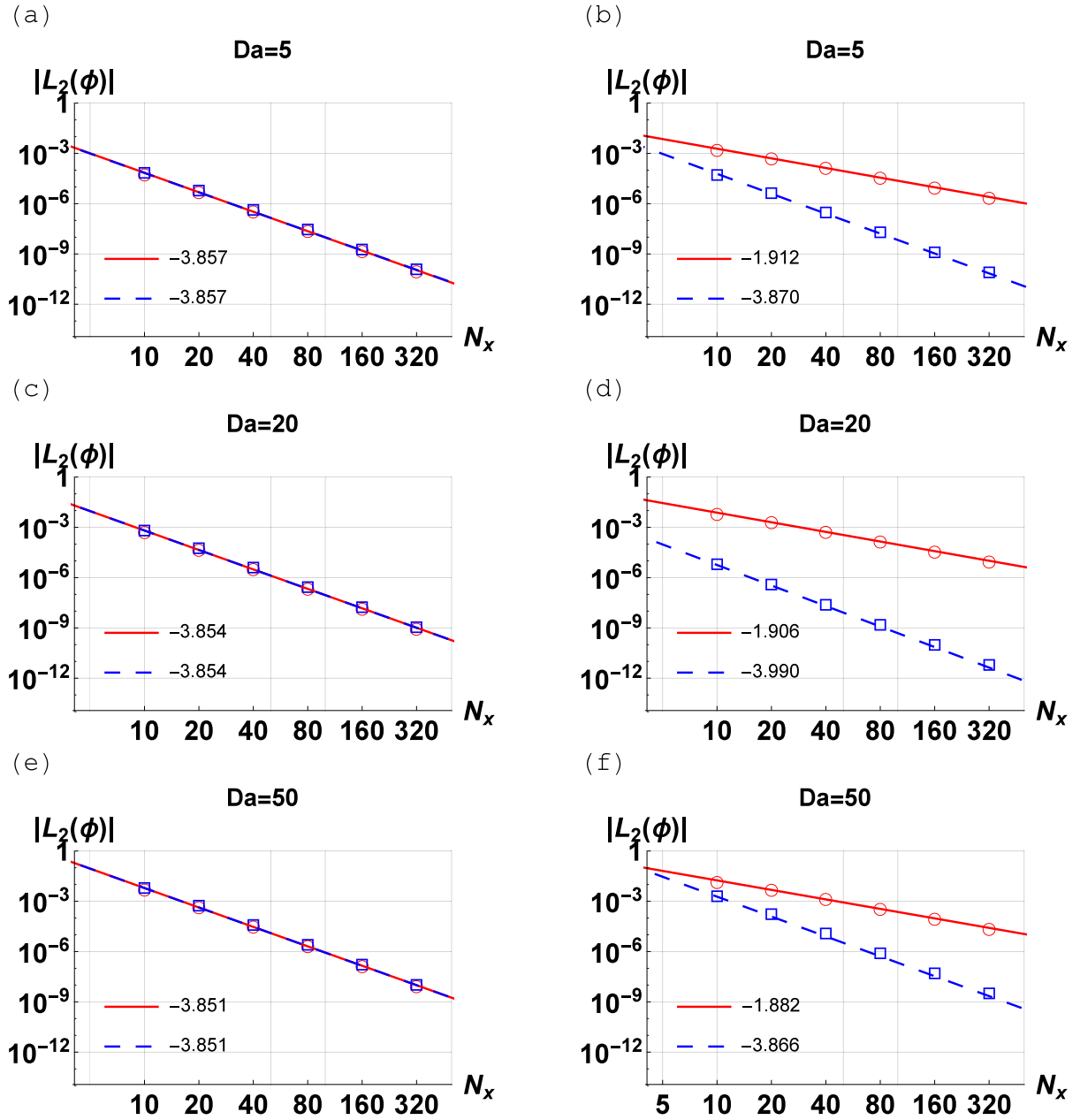
(a)

(b)

(c)

(d)

(e)

(f)

Fig. 5. Benchmark 1. Mesh convergence solutions for $t^\star = 0.05$ along various Da numbers. Red continuous line with circle marks: SF scheme. Blue dashed line with square marks: IF scheme. Incepts quantify the converge rates given by the slopes of fitting lines obtained from linear regression. Panels (a), (c) and (e): $s^- = 1$ and $s^+ = 42/41$. Panels (b), (d) and (f): $s^- = 1.1148342422560822$ and $s^+ = 1$.

the first three time levels. They are prescribed here recurring to the analytical solutions, which are provided below for each case considered, although they could be also determined numerically, through an auxiliary numerical scheme. As for the spatial discretization, computational nodes are set at the edges of computational cells $x_j = j\,\Delta x$ with $j = 0, \ldots, N_x$, and boundary conditions are prescribed at the end points of the computational domain, $x_0 = 0$ and $x_{N_x} = N_x\,\Delta x$. The spatial and temporal discretization steps are defined as $\Delta x = 2\,\ell / N_x$ and $\Delta t = \Delta x^2$, respectively.

This finite-difference based implementation described above is equivalent to the LBM-TRT method implementation, using the LSOB model, given by Eq. (34), as boundary scheme whereas the initialization procedure could use the analytical reconstruction of the LBM-TRT populations for the first three time levels, recurring to, for example, the fourth-order population reconstruction formulas presented in the work [47].

The accuracy of numerical solutions will be determined based on:

$$|L_2(\phi)| = \sqrt{\sum_j \left(\phi_j^n - \phi_j^{n\,(\text{analy})}\right)^2 \Big/ \sum_j (\phi_j^{n\,(\text{analy})})^2} \tag{70}$$

where sums are taken over the full computational domain at time level n, determined as $n = t^\star \ell^2 / (D\,\Delta t) = t^\star\, 4\, N_x^2 / \epsilon$ where $\ell = N_x\,\Delta x / 2$.

6.1. Benchmark 1. Time decaying unbounded concentration wave

Benchmark 1 solves Eq. (1), with $\mathcal{M} = 0$, subject to inhomogeneous initial and periodic boundary conditions given by:

$$\phi(-1 < x^\star < 1, t^\star = 0) = \cos(\pi x^\star) + \sin(\pi x^\star), \tag{71a}$$

$$\phi(x^\star = \pm 1, t^\star \geq 0) = -\exp\left(-t^\star\left(\text{Da} + \pi^2\right)\right). \tag{71b}$$

Table 2
Main characteristics of the benchmark tests considered in this study.

	Constant mass source	Initial condition	Boundary conditions	Solution
Benchmark 1	No	Inhomogeneous	Periodic	Eq. (72)
Benchmark 2	No	Inhomogeneous	Homogeneous	Eq. (74)
Benchmark 3	No	Homogeneous	Inhomogeneous	Eq. (76)
Benchmark 4	Yes	Homogeneous	Homogeneous	Eq. (78)

Benchmark 1 solution is:

$$\phi(x^\star, t^\star) = \left(\cos(\pi x^\star) + \sin(\pi x^\star)\right) \exp\left(-t^\star \left(\mathrm{Da} + \pi^2\right)\right). \tag{72}$$

Fig. 4 illustrates the periodic wave solutions $\phi(x^\star, t^\star)$, described by Eq. (72), along the reaction–diffusion regimes $\mathrm{Da} = \{5, 20, 50\}$, fixating $t^\star = 0.05$. This figure shows the larger is the Da regime, i.e. the larger is the dominance of reaction over diffusion, the faster is the decay of the concentration wave towards a uniform zero state.

Fig. 5 shows the evolution of the SF and IF numerical accuracy with the mesh resolution, for the Da regimes considered in Fig. 4. Fig. 5 plots (a), (c) and (e) consider the relaxation rates $s^- = 1$ and $s^+ = 42/41$, which is the solution of Eq. (62) for $\epsilon = 0.1$. This case makes the SF scheme formally $\mathcal{O}(\Delta t^2, \Delta x^4)$ accurate. With this relaxation choice SF and IF schemes have a similar discretization structure. Fig. 5 plots (b), (d) and (f) consider the relaxation rates $s^- = 1.1148342422560822$ and $s^+ = 1$, which is the solution of Eq. (69) for $\epsilon = 0.1$ that makes the IF scheme formally $\mathcal{O}(\Delta t^2, \Delta x^4)$ accurate, although it maintains the $\mathcal{O}(\Delta t, \Delta x^2)$ accuracy in the SF scheme. In conclusion, the numerical results here presented confirm the theoretical conclusions, regarding the order of accuracy of each model, for every Da regime and also for every $t^\star$, although the dependence on $t^\star$ is not discussed in the manuscript.

6.2. Benchmark 2. Time decaying bounded concentration wave

Benchmark 2 solves Eq. (1), with $\mathcal{M} = 0$, subject to inhomogeneous initial and prescribed homogeneous boundary conditions given by:

$$\phi(-1 < x^\star < 1, t^\star = 0) = \sin(\tfrac{\pi}{2} x^\star), \tag{73a}$$

$$\phi(x^\star = \pm 1, t^\star \geq 0) = 0. \tag{73b}$$

Benchmark 2 solution is:

$$\phi(x^\star, t^\star) = \sin(\tfrac{\pi}{2} x^\star) \exp\left(-t^\star \left(\mathrm{Da} + \tfrac{\pi^2}{4}\right)\right). \tag{74}$$

Fig. 6 illustrates the bounded wave solutions $\phi(x^\star, t^\star)$, described by Eq. (74), along the reaction–diffusion regimes $\mathrm{Da} = \{5, 20, 50\}$, fixating $t^\star = 0.05$. Once again, the decaying rate towards a uniform zero state is faster the larger is the Da regime.

Fig. 7 shows the evolution of the SF and IF numerical accuracy with the mesh resolution, for the Da regimes considered in Fig. 6. Fig. 7 plots (a), (c) and (e) consider the relaxation rates $s^- = 1$ and $s^+ = 42/41$, which is the solution of Eq. (62) for $\epsilon = 0.1$, which makes the SF scheme formally $\mathcal{O}(\Delta t^2, \Delta x^4)$ accurate and equal to IF. Fig. 7 plots (b), (d) and (f) consider the relaxation rates $s^- = 1.1148342422560822$ and $s^+ = 1$, which makes the IF scheme formally $\mathcal{O}(\Delta t^2, \Delta x^4)$ accurate, although it maintains the $\mathcal{O}(\Delta t, \Delta x^2)$ accuracy in the SF scheme. These conclusions are numerically verified in Fig. 7 for every Da regime (and also for every $t^\star$, although not shown here).

6.3. Benchmark 3. Time growing concentration towards boundary value

Benchmark 3 solves Eq. (1), with $\mathcal{M} = 0$, subject to homogeneous initial and prescribed inhomogeneous boundary conditions given by:

$$\phi(-\ell < x < \ell, t = 0) = 0, \tag{75a}$$
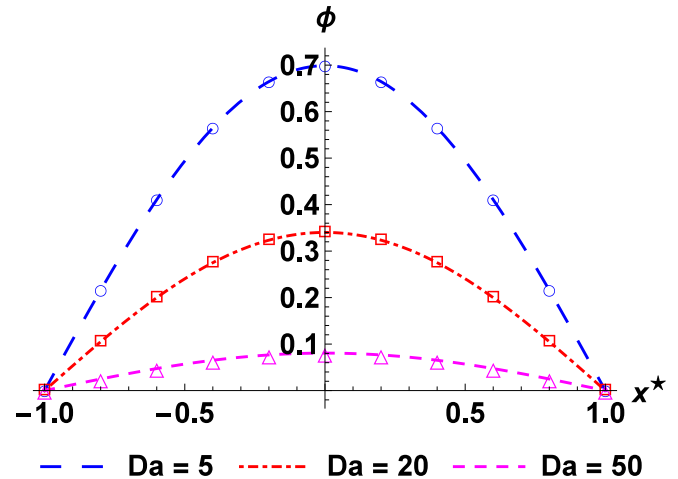
$$\phi(x = \pm\ell, t \geq 0) = \phi_0. \tag{75b}$$

Fig. 6. Benchmark 2. Time decaying bounded wave with $t^\star = 0.05$, $\mathcal{D} = 0.1$, $N_x = 10$, $\Delta x = 1$, $\ell = N_x \Delta x/2 = 5$. Continuous lines depict the analytical solutions, given by Eq. (74). Markers indicate the nodal values obtained with SF scheme, using $s^- = 1$ and $s^+ = 42/41$.

Benchmark 3 solution is:

$$\phi(x^\star, t^\star) = \phi_0 \left[\frac{\cosh\left(x^\star \sqrt{\mathrm{Da}}\right)}{\cosh\left(\sqrt{\mathrm{Da}}\right)} \right.$$

$$- \frac{4}{\pi} \sum_{n=0}^{\infty} \frac{(-1)^n}{(2n+1)} \frac{\cos\left(x^\star \frac{(2n+1)\pi}{2}\right)}{\left(1 + \frac{4\,\mathrm{Da}}{(2n+1)^2 \pi^2}\right)}$$

$$\left. \times \exp\left(-t^\star \left(\mathrm{Da} + \frac{(2n+1)^2 \pi^2}{4}\right)\right) \right]. \tag{76}$$

In this work the infinite series in Eq. (76) is computed with 100 terms.

Fig. 8 illustrates the bounded time growing solutions $\phi(x^\star, t^\star)$, described by Eq. (76), along the reaction–diffusion regimes $\mathrm{Da} = \{5, 20, 50\}$, fixating $t^\star = 0.05$. Larger Da regimes result in ϕ profiles with narrow boundary layers in both transient and steady regimes. The steady solution is $\phi(x^\star) = \phi_0 \cosh\left(x^\star \sqrt{\mathrm{Da}}\right) / \cosh\left(\sqrt{\mathrm{Da}}\right)$.

Now, let us examine the quality of the numerical solutions supplied by the LBM-TRT with the SF scheme. Fig. 9 compares this scheme for two mesh resolutions $N_x = 10$ and $N_x = 20$ versus the analytical solution, given by Eq. (76), taking $\mathrm{Da} = 500$ (i.e. the ϕ profile with very steep boundary layers) and $t^\star = 0.05$. Owing to the very sharp gradients near boundaries, a spatial resolution of $N_x = 10$ inevitably places all grid nodes outside the boundary layers. Thus, it not possible to explicitly resolve these features with this grid resolution. To make matters worse, the source discretization artefact also comes into play with a very high magnitude, in this case, which causes the overshoots in the solution profile an undesirable artefact. The traditional way to clean these defects is to increase the grid resolution. For example, doubling the grid resolution to $N_x = 20$ significantly improves the solution quality, but at the obvious cost of a higher computational overhead,
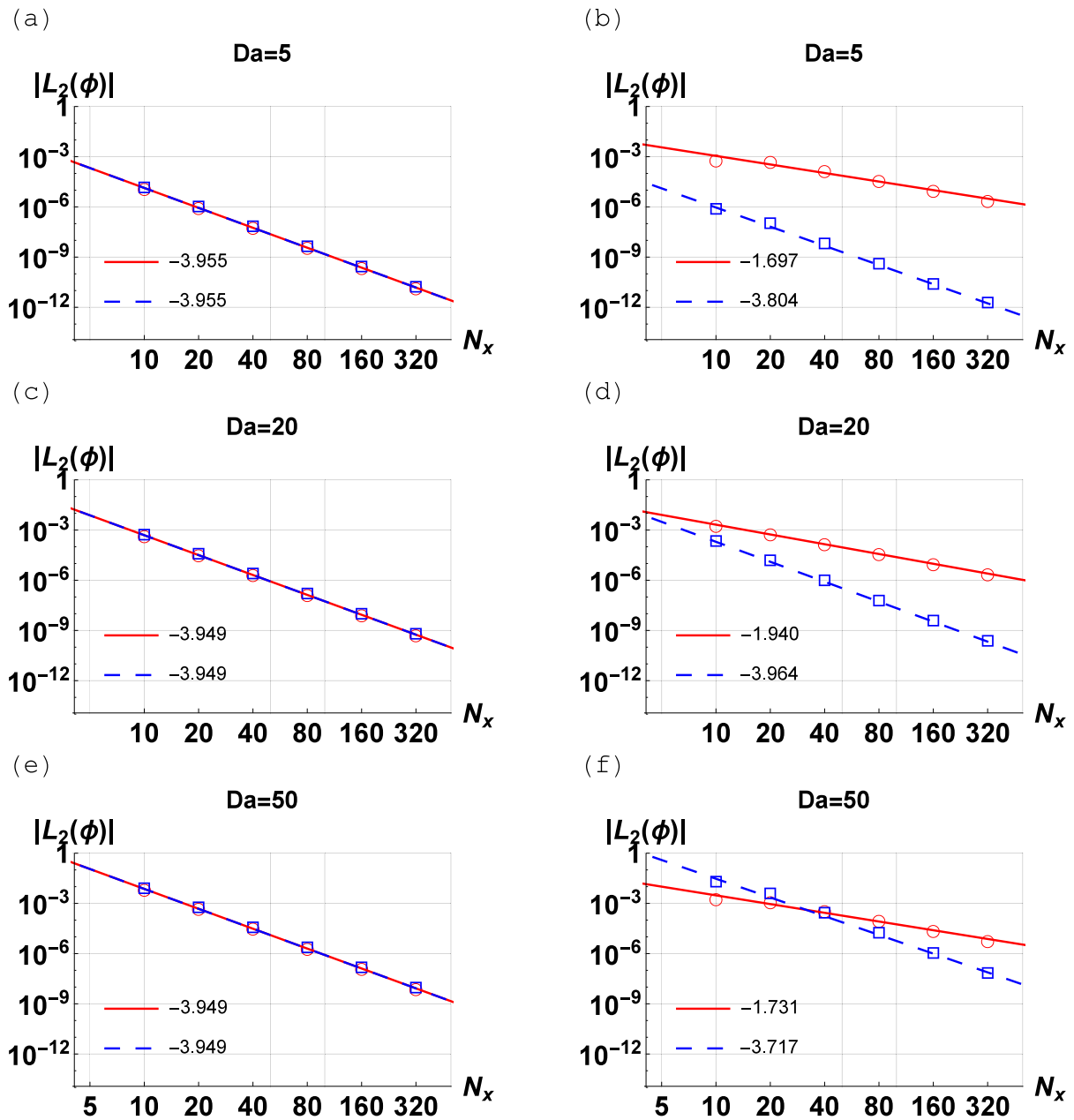
Fig. 7. Benchmark 2. Mesh convergence solutions for $t^\star = 0.05$ along various Da numbers. Red continuous line with circle marks: SF scheme. Blue dashed line with square marks: IF scheme. Incepts quantify the converge rates given by the slopes of fitting lines obtained from linear regression. Panels (a), (c) and (e): $s^- = 1$ and $s^+ = 42/41$. Panels (b), (d) and (f): $s^- = 1.1148342422560822$ and $s^+ = 1$.

which for large scale problem may not be feasible. For that reason, the IF scheme is worth exploration, a task that will be pursued next.

To investigate the performance of the IF scheme, let us consider both the original steady IF formulation, given by Eq. (27), and the new transient one, given by Eq. (65). Fig. 10 compares the quality of numerical solutions, given by SF, IF [Unsteady] and IF [Steady] schemes, versus the analytical solution, given by Eq. (76), taking Da = 500 and $t^\star = 0.05$ as in the previous case. Although the problem is time-dependent, let us assume the steady-state formula, given by Eq. (24), is valid, which implies that the diffusion coefficient correction is $\delta = -2.35337$. Under these circumstances, the effective diffusion coefficient becomes negative, which explains the overshoots in the SF profiles, as already pointed out in Fig. 9. Alternatively, the IF scheme (with both unsteady and steady formulations) manages to mitigate these overshoots in the solution. Nonetheless, during the transient stage of the solution, the IF [Unsteady] scheme, given by Eq. (65), substantially

improves the quality and the accuracy of the solution, see caption in Fig. 10. In fact, the IF [Unsteady] with $N_x = 10$ is even more accurate than the SF with $N_x = 20$, i.e. using twice the grid resolution. For that reason, the IF scheme, in its unsteady formulation, seems the preferred choice, which supports the theoretical analysis. On this basis, only the IF [Unsteady] scheme will be considered in the mesh refinement analysis discussed next.

Concerning the accuracy supported by the two source implementations considered here, Fig. 11 shows the evolution of the SF and IF numerical error with the mesh resolution for the same Da regimes of Fig. 8. Fig. 7 plots (a), (c) and (e) consider the relaxation rates $s^- = 1$ and $s^+ = 42/41$, which is the solution of Eq. (62) for $\epsilon = 0.1$ that makes the SF scheme formally $\mathcal{O}(\Delta t^2, \Delta x^4)$ accurate. This relaxation choice makes SF and IF schemes to have a similar discretization structure. Fig. 7 plots (b), (d) and (f) consider the relaxation rates $s^- = 1.1148342422560822$ and $s^+ = 1$, which is the solution of Eq. (69)
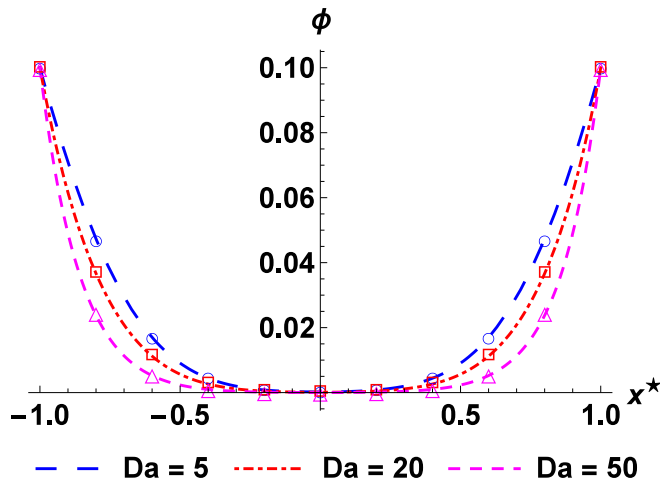
Fig. 8. Benchmark 3. Time growing concentration towards boundary value with $t^\star = 0.05$, $D = 0.1$, $N_x = 10$, $\Delta x = 1$, $\ell = N_x \Delta x/2 = 5$ and $\phi_0 = 0.1$. Continuous lines depict the analytical solutions, given by Eq. (76). Markers indicate the nodal values obtained with SF scheme, using $s^- = 1$ and $s^+ = 42/41$.
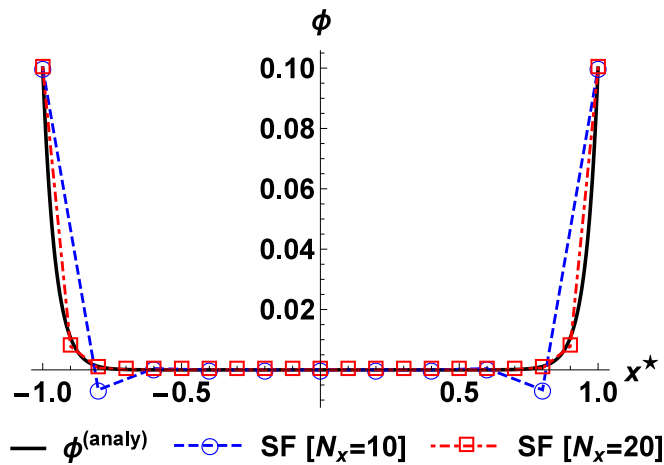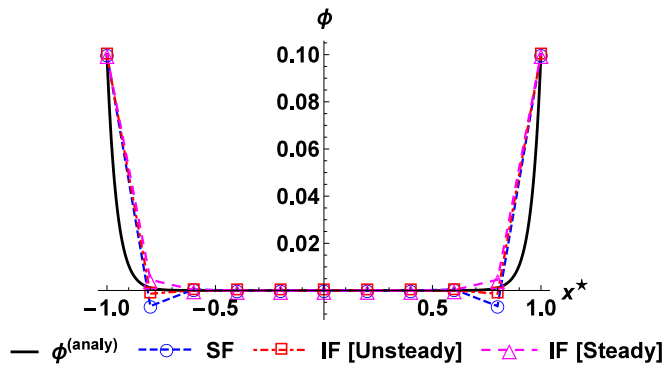

Fig. 9. Benchmark 3. Time growing concentration towards boundary value with Da = 500, $t^\star = 0.05$, $D = 0.071$, and $\phi_0 = 0.1$, with $\Delta x = 1$ and $\ell = N_x \Delta x/2$ where N_x varies. Continuous black line depicts the analytical solutions, given by Eq. (76). Markers indicate the nodal values with the SF scheme, using $s^- = 1.1148342422560822$ and $s^+ = 1$, with different N_x mesh resolutions. Accuracies: $|L_2(\phi)| = 0.0777$ with $N_x = 10$ and $|L_2(\phi)| = 0.0292$ with $N_x = 20$.

Fig. 10. Benchmark 3. Time growing concentration towards boundary value with Da = 500, $t^\star = 0.05$, $D = 0.071$, $N_x = 10$, $\Delta x = 1$, $\ell = N_x \Delta x/2 = 5$ and $\phi_0 = 0.1$. Continuous black line depicts the analytical solutions, given by Eq. (76). Markers indicate the nodal values with SF, IF [Unsteady] and IF [Steady] schemes, using $s^- = 1.1148342422560822$ and $s^+ = 1$. Accuracies: $|L_2(\phi)| = 0.0777$ in SF, in $|L_2(\phi)| = 0.0251$ in IF [Unsteady], and $|L_2(\phi)| = 0.0342$ in IF [Steady].

for $\epsilon = 0.1$ that makes the IF scheme formally $\mathcal{O}(\Delta t^2, \Delta x^4)$ accurate, although the SF scheme remains formally $\mathcal{O}(\Delta t, \Delta x^2)$ accurate. These theoretical conclusions are numerically verified in Fig. 11.

6.4. Benchmark 4. Time growing concentration generated by constant source term

Benchmark 4 solves Eq. (1), $\mathcal{M} = \text{const} \neq 0$, subject to homogeneous initial and prescribed homogeneous boundary conditions given by:

$$\phi(-\ell < x < \ell, t = 0) = 0, \tag{77a}$$

$$\phi(x = \pm\ell, t \geq 0) = 0. \tag{77b}$$

Benchmark 4 solution is:

$$\phi(x^\star, t^\star) = \frac{\mathcal{M}}{\kappa} \left[1 - \frac{\cosh\left(x^\star \sqrt{\text{Da}}\right)}{\cosh\left(\sqrt{\text{Da}}\right)} \right.$$

$$- \frac{4}{\pi} \sum_{n=0}^{\infty} \frac{(-1)^n}{(2n+1)} \frac{\cos\left(x^\star \frac{(2n+1)\pi}{2}\right)}{\left(1 + \frac{(2n+1)^2 \pi^2}{4\,\text{Da}}\right)} \tag{78}$$

$$\left. \times \exp\left(-t^\star \left(\text{Da} + \frac{(2n+1)^2 \pi^2}{4}\right)\right) \right].$$

In this work the infinite series in Eq. (78) is computed with 100 terms.

Fig. 12 illustrates the time growing concentration solutions, generated by constant source term, $\phi(x^\star, t^\star)$, described by Eq. (78), along the reaction–diffusion regimes Da = {5, 20, 50}, fixating $t^\star = 0.05$. Larger Da regimes retard the growth of ϕ profiles in both transient and steady regimes. The steady solution is $\phi(x^\star) = \frac{\mathcal{M}}{\kappa} \left[1 - \cosh\left(x^\star \sqrt{\text{Da}}\right) / \cosh\left(\sqrt{\text{Da}}\right) \right]$.

The quality of the numerical solutions supplied by the LBM-TRT with the SF scheme is now investigated for this benchmark test. Fig. 13 compares this scheme output for two mesh resolutions $N_x = 10$ and $N_x = 20$ versus the analytical solution, given by Eq. (78), taking Da = 500 (i.e. a ϕ profile with very steep boundary layers) and $t^\star = 0.05$. Once again, a coarse grid resolution like $N_x = 10$ is not able to explicitly resolve the boundary layers, which alongside with the source discretization artefact produces the observed overshoots in the solution profile. By doubling the grid resolution to $N_x = 20$, the solution quality can be improved, but the IF scheme may offer a more elegant alternative.

Fig. 14 compares the quality of the SF, the IF [Unsteady], Eq. (65), and the IF [Steady], Eq. (27), schemes, considering Da = 500 and $t^\star = 0.05$. The SF solution features overshoots, while the IF scheme (using both unsteady and steady formulations) mitigates this defect, by correcting the diffusion coefficient value, although the IF [Steady] scheme is slightly more over-dissipative during the transient regime. Overall, the IF [Unsteady] scheme, given by Eq. (65), tends to exhibit the best quality and accuracy among the tested schemes. Although, it is slightly less accurate in this case, the IF [Unsteady] scheme with $N_x = 10$ reaches virtually the same level of accuracy of the SF with $N_x = 20$. Due to its superior characteristics, the mesh refinement analysis presented next will only focus on the IF [Unsteady] formulation.

Fig. 15 shows the evolution of the numerical error along with the mesh resolution for the Da regimes considered in Fig. 12. Fig. 11 plots (a), (c) and (e) consider the relaxation rates $s^- = 1$ and $s^+ = 42/41$, which is the solution of Eq. (62) for $\epsilon = 0.1$ that makes the SF scheme formally $\mathcal{O}(\Delta t^2, \Delta x^4)$ accurate. This relaxation choice makes SF and IF schemes to have a similar discretization structure. Fig. 11 plots (b), (d) and (f) consider the relaxation rates $s^- = 1.1148342422560822$ and $s^+ = 1$, which is the solution of Eq. (69) for $\epsilon = 0.1$ that makes the IF scheme formally $\mathcal{O}(\Delta t^2, \Delta x^4)$ accurate, whereas the SF scheme maintains the $\mathcal{O}(\Delta t, \Delta x^2)$ accuracy.
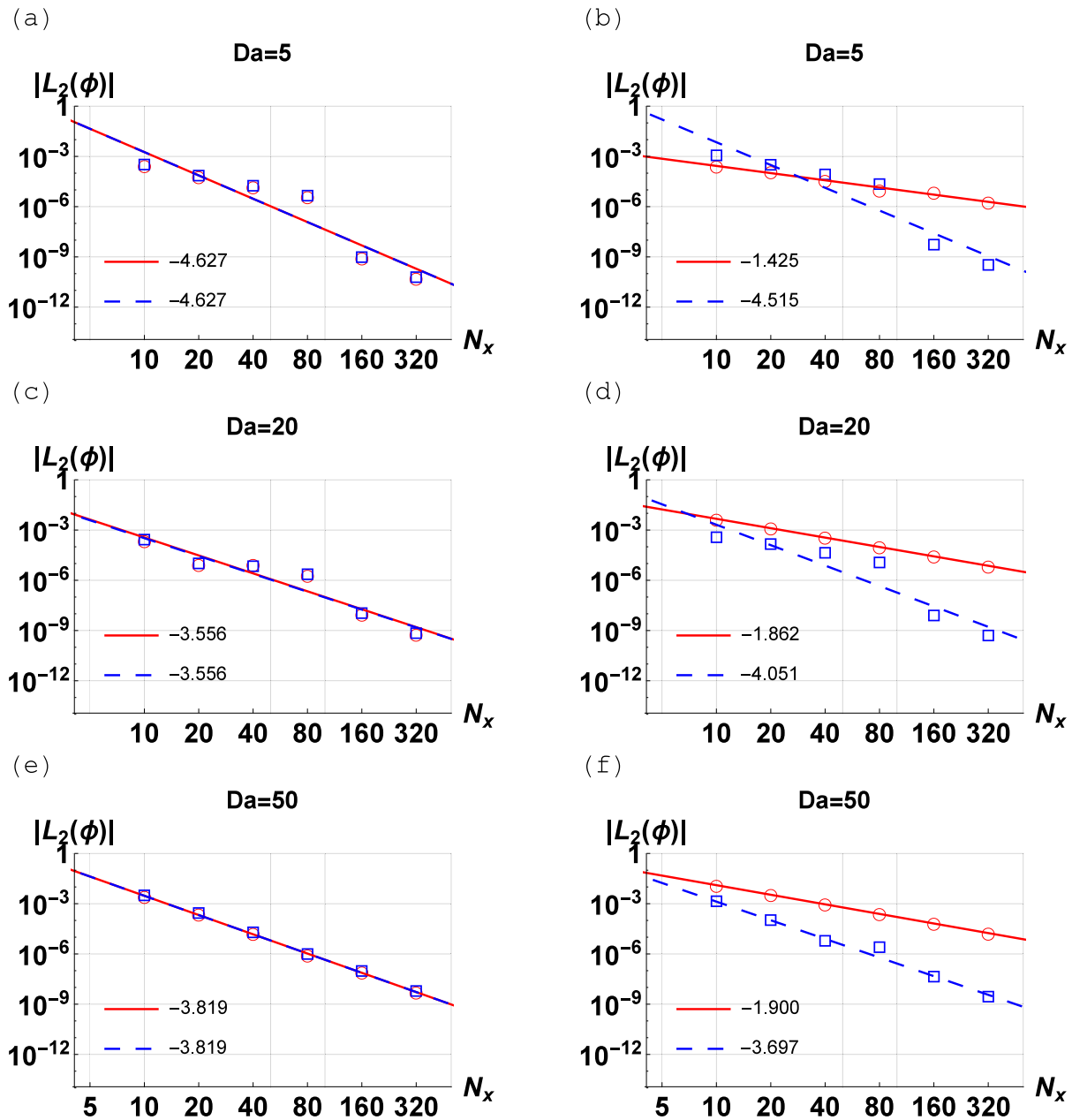
Fig. 11. Benchmark 3. Mesh convergence solutions for $t^\star = 0.05$ along various Da numbers. Red continuous line with circle marks: SF scheme. Blue dashed line with square marks: IF scheme. Incepts quantify the converge rates given by the slopes of fitting lines obtained from linear regression. Panels (a), (c) and (e): $s^- = 1$ and $s^+ = 42/41$. Panels (b), (d) and (f): $s^- = 1.1148342422560822$ and $s^+ = 1$.

7. Conclusions

This work performed a detailed numerical analysis on the LBM-TRT modelling of the one-dimensional reaction–diffusion equation, with special attention paid to the discrete effects on the source term representation. For this study, three main tasks were undertaken. First, the discrete structure of the LBM-TRT scheme with a source, under the D1Q3 lattice, was derived and showed to approximate Eq. (1) as a *four-level explicit finite difference scheme*, where the external source contributes to the overall discretization by modifying the scheme coefficients. In the steady-state limit, this scheme reduces to a second-order finite difference approximation, where all coefficients can be merged

to form an effective diffusion coefficient. This effective diffusion coefficient differs from the assigned (physical) one due to numerical artefacts coming from the source term discretization. Whenever the TRT relaxation parameter obeys $\Lambda < 3/8$, this numerical artefact becomes negative and the solution is susceptible to an oscillatory behaviour. Surprisingly, despite how negative the scheme diffusion coefficient is, the LBM-TRT solution appears to always converge towards a steady state. Hence, the second task of this work aimed at explaining this result. For that, a rigorous stability analysis was performed over the LBM-TRT scheme with a source. The outcome of this analysis proved the *scheme unconditional stability*, within the range of parameters typically considered in LBM. The third and final task of this work examined the
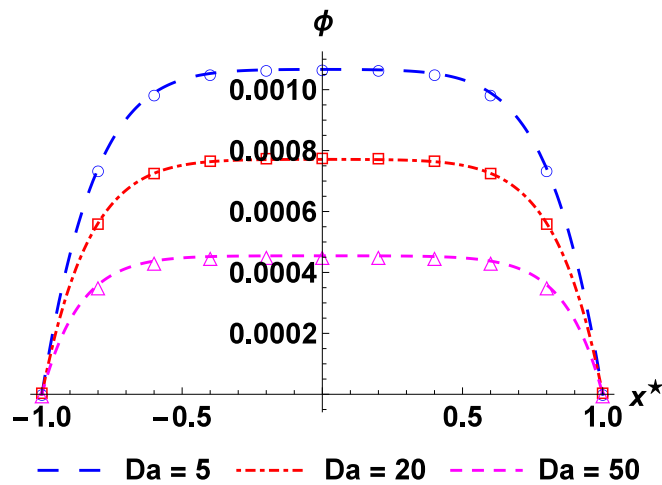
Fig. 12. Benchmark 4. Time growing concentration generated by constant source term with $t^\star = 0.05$, $\mathcal{D} = 0.1$, $N_x = 10$, $\Delta x = 1$, $\ell = N_x \Delta x/2 = 5$ and $\mathcal{M} = 0.01$. Continuous lines depict the analytical solutions, given by Eq. (78). Markers indicate the nodal values obtained with SF scheme, using $s^- = 1$ and $s^+ = 42/41$.
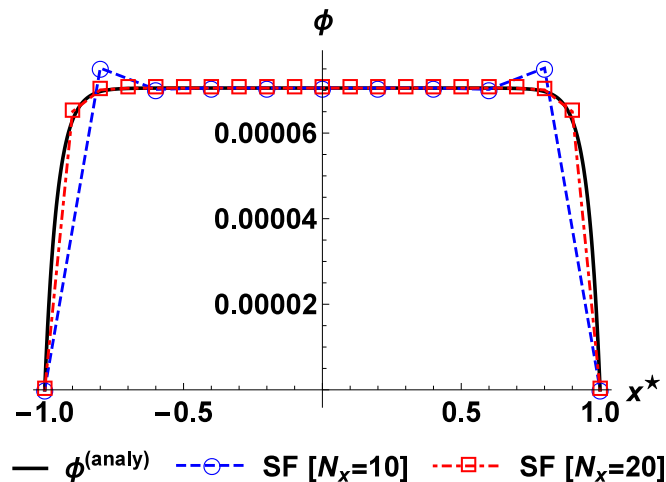

Fig. 13. Benchmark 4. Time growing concentration generated by constant source term with $Da = 500$, $t^\star = 0.05$, $\mathcal{D} = 0.07$ and $\mathcal{M}_0 = 0.1$, with $\Delta x = 1$ and $\ell = N_x \Delta x/2$ where N_x varies. Continuous black line depicts the analytical solutions, given by Eq. (78). Markers indicate the nodal values with the SF scheme, using $s^- = 1.1148342422560822$ and $s^+ = 1$, with different N_x mesh resolutions. Accuracies: $|L_2(\phi)| = 0.0367$ with $N_x = 10$ and $|L_2(\phi)| = 0.0096$ with $N_x = 20$.

Fig. 14. Benchmark 4. Time growing concentration generated by constant source term with $Da = 500$, $t^\star = 0.05$, $\mathcal{D} = 0.07$, $N_x = 10$, $\Delta x = 1$, $\ell = N_x \Delta x/2 = 5$ and $\mathcal{M}_0 = 0.1$. Continuous black line depicts the analytical solutions, given by Eq. (78). Markers indicate the nodal values with SF, IF [Unsteady] and IF [Steady] schemes, using $s^- = 1.1148342422560822$ and $s^+ = 1$. Accuracies: $|L_2(\phi)| = 0.0367$ in SF, in $|L_2(\phi)| = 0.0118$ in IF [Unsteady], and $|L_2(\phi)| = 0.0162$ in IF [Steady].

truncation structure of the LBM-TRT scheme with a source. The end purpose was to find ways to improve the scheme accuracy when solving Eq. (1). For that, two strategies were devised. The first one, based on the standard force (SF) formulation, determined how to fixate the free parameters of the numerical scheme in order to reach an *improved* $\mathcal{O}(\Delta t^2, \Delta x^4)$ *accuracy*. The second procedure studied an alternative strategy to achieve this level of accuracy, but without constraining all free parameters to fixed values. To this end, it was proposed an improved force (IF) formulation, based on the redefinition of the TRT relaxation parameters, adapting the original ideas of the work [65], but applied to a time-dependent setting. This IF strategy intended to remove the leading order source term artefact from the LBM-TRT scheme, and by doing so it was able: (i) to reach the $\mathcal{O}(\Delta t^2, \Delta x^4)$ accuracy with greater flexibility, (ii) to strongly mitigate oscillatory-like artefacts on the numerical solutions, without being too dissipative, and (iii) to
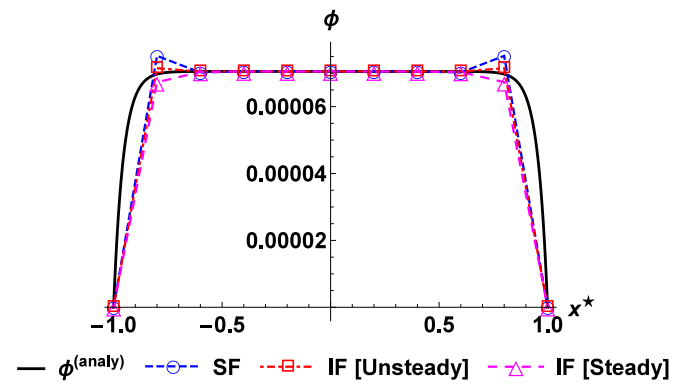
conserve the unconditional stability properties of the standard model, while virtually requiring no extra effort in terms of numerical overhead and implementation. At last, these findings were examined throughout diverse numerical tests, which confirmed the main theoretical results developed in this study. As future work, it is planned to incorporate the effect of fluid advection in the theoretical analysis, and examine how the results here obtained and the models here proposed extend to two- and three-dimensional problems [72,73,75]. Concerning this last point, one should keep in mind the important conclusions reached by previous studies on the effect of velocity-dependent sources in the LBM modelling of fluid flows, namely porous media flows governed by steady Stokes–Brinkman equations [20,65,76], which revealed that the discretization of velocity-dependent sources introduces anisotropic errors in multi-dimensions. Hence, the next logical step shall be to understand whether this artefact, that results from the insufficient isotropy of the discrete velocity model, also translates to time-dependent reaction–diffusion problems in higher dimensions. An answer to this question is not immediate, requiring a dedicated analysis, since advection–diffusion models are typically subject to lattice constraints that are not as severe as in the case of fluid flow models in LBM.

CRediT authorship contribution statement

Goncalo Silva: Conceptualization, Investigation, Methodology, Software, Visualization, Writing – original draft, Writing – review & editing, Validation.

Declaration of competing interest

The authors declare that they have no known competing financial interests or personal relationships that could have appeared to influence the work reported in this paper.

Data availability

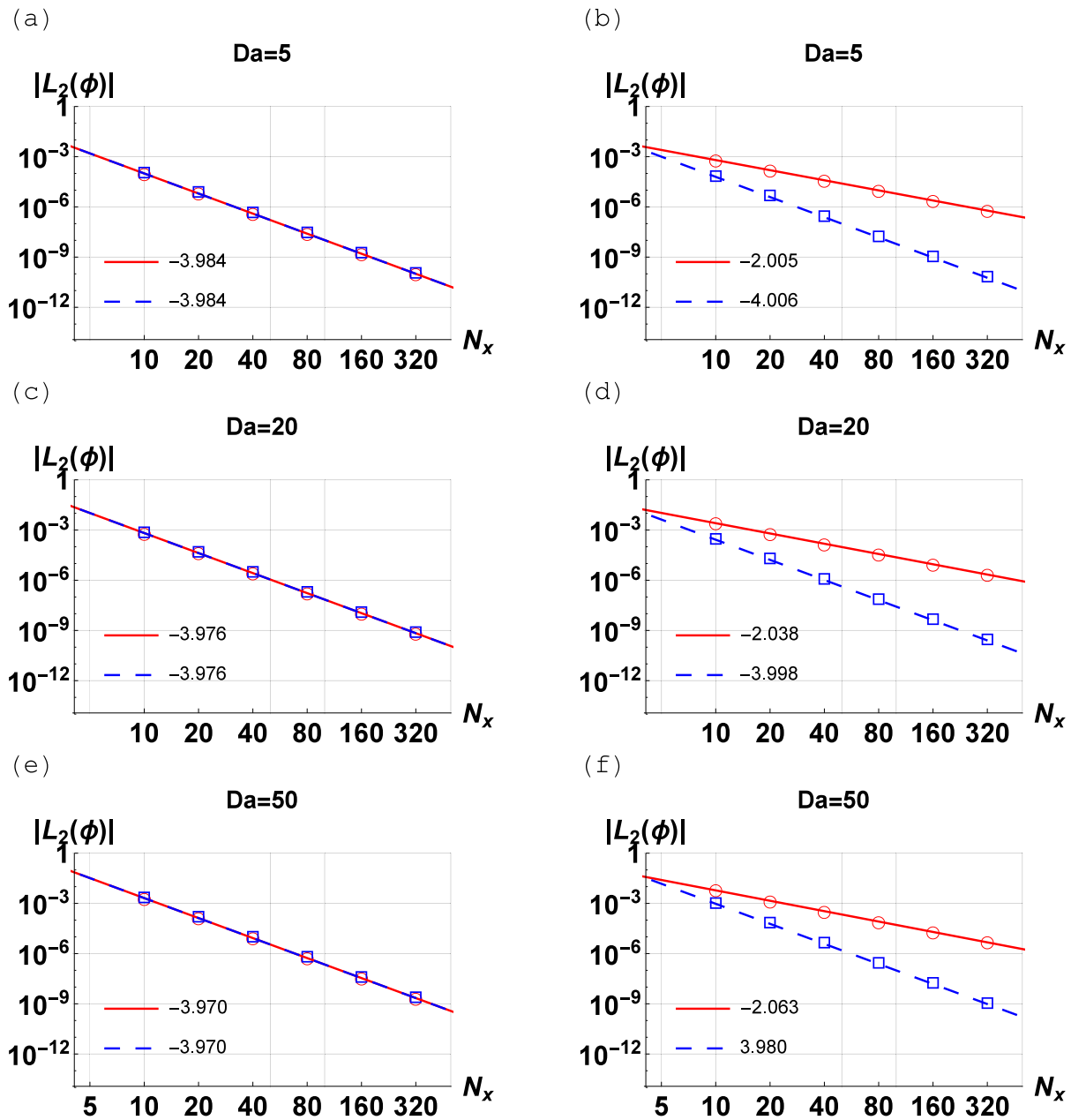Data will be made available on request

Acknowledgements

Fig. 15. Benchmark 4. Mesh convergence solutions for $t^\star = 0.05$ along various Da numbers. Red continuous line with circle marks: SF scheme. Blue dashed line with square marks: IF scheme. Incepts quantify the converge rates given by the slopes of fitting lines obtained from linear regression. Panels (a), (c) and (e): $s^- = 1$ and $s^+ = 42/41$. Panels (b), (d) and (f): $s^- = 1.1148342422560822$ and $s^+ = 1$.

References

[1] Farlow SJ. Partial differential equations for scientists and engineers. 1st ed.. Courier Corporation; 2012.

[2] Crank J. The mathematics of diffusion. 2nd ed.. Oxford University Press; 1980.

[3] Carslaw HS, Jaeger JC. Conduction of heat in solids. 2nd ed.. Oxford University Press; 1986.

[4] Mavroudi M, Kaldis SP, Sakellaropoulos GP. A study of mass transfer resistance in membrane gas–liquid contacting processes. J Membr Sci 2006;272:103–15.

[5] Nagy E, Lepossa A, Prettl Z. Mass transfer through a biocatalytic membrane reactor. Ind Eng Chem Res 2012;51(4):1635–46.

[6] Suryanarayana NV. Transient response of straight fins: Part II. J Heat Transfer 1976;98(2):324–6.

[7] Estrada-Gasca CA, Cooble MH, Garcia GA. One-dimensional non-linear transient heat conduction in nuclear waste repositories. Eng Comput 1991;8(4):345–60.

[8] Chu M, Kitanidis P, McCarty P. Dependence of lumped mass transfer coefficient on scale and reactions kinetics for biologically enhanced NAPL dissolution. Adv Water Resour 2007;30(6):1618–29.

[9] Fletcher C. Computational techniques for fluid dynamics, Vol. 1. 2nd ed.. Springer-Verlag Berlin Heidelberg; 1998.

[10] Yu Z, Wei Z, Chenhui Z, Yulan W. Numerical solution of a coupled reaction–diffusion model using barycentric interpolation collocation method. Therm Sci 2020;24(4):2561–7.

[11] Andersen P, Evje S. A model for reactive flow in fractured porous media. Chem Eng Sci 2016;145:196–213.

[12] Carvalho AN, Cuminato JA. Reaction–diffusion problems in cell tissues. J Dynam Differential Equations 1997;9(1):93–131.

[13] Iida M, Ninomiya H, Yamamoto H. A review on reaction–diffusion approximation. J Elliptic Parabol Equ 2018;4:565–600.

[14] Chen S, Doolen G. Lattice Boltzmann method for fluid flows. Ann Rev Fluid Mech 1998;30:329–64.

[15] Aidun CK, Clausen JR. Lattice-Boltzmann method for complex flows. Ann Rev Fluid Mech 2010;42:439–72.

[16] Krüger T, Kusumaatmaja H, Kuzmin A, Shardt O, Silva G, Viggen EM. The lattice Boltzmann method - principles and practice. 1st ed.. Springer International Publishing; 2016.

[17] Succi S. The lattice Boltzmann equation: for complex states of flowing matter. Oxford University Press; 2018.

[18] Marie S, Ricot D, Sagaut P. Comparison between lattice Boltzmann method and Navier–Stokes high-order schemes for computational aeroacoustics. J Comput Phys 2009;228(4):1056–70.

[19] Peng Y, Liao W, Luo L-S, Wang L-P. Comparison of the lattice Boltzmann and pseudo-spectral methods for decaying turbulence: Low-order statistics. Comput & Fluids 2010;39(4):568–91.

[20] Silva G, Talon L, Ginzburg I. Low-and high-order accurate boundary conditions: From Stokes to Darcy porous flow modeled with standard and improved Brinkman lattice Boltzmann schemes. J Comput Phys 2017;335:50–83.

[21] Silva G. Consistent lattice Boltzmann modeling of low-speed isothermal flows at finite Knudsen numbers in slip-flow regime. II. Application to curved boundaries. Phys Rev E 2018;98:023302.

[22] He X, Zou Q, Luo L-S, Dembo M. Lattice Boltzmann Model for the Incompressible Navier-Stokes Equation. J Stat Phys 1997;88:927–44.

[23] Lallem P, Luo L-S, Krafczyk M, Yong W-A. The lattice Boltzmann method for nearly incompressible flows. J Comput Phys 2021;431:109713.

[24] Ginzburg I. Equilibrium-type and link-type lattice Boltzmann models for generic advection and anisotropic-dispersion equation. Adv Water Resour 2005;28:1171–95.

[25] Chopard B, Falcone JL, Latt J. The lattice Boltzmann advection-diffusion model revisited. Eur Phys J Spec Top 2009;171:245–9.

[26] Shi B, Guo Z. Lattice Boltzmann model for nonlinear convection–diffusion equations. Phys Rev E 2009;79:016701.

[27] Chai Z, He N, Guo Z, Shi B. Lattice Boltzmann model for high-order nonlinear partial differential equations. Phys Rev E 2018;97:013304.

[28] Chai ZH, Shi BC. A novel lattice Boltzmann model for the Poisson equation. Appl Math Model 2008;32:2050–8.

[29] Zhang J, Yan G. A lattice Boltzmann model for the Burgers–Fisher equation. Chaos 2010;20:023129.

[30] Zhang J, Yan G. Lattice Boltzmann model for the complex Ginzburg–Landau equation. Phys Rev E 2010;81:066705.

[31] Zhong LH, Feng SD, Dong P, Gao ST. Lattice Boltzmann schemes for the nonlinear Schrödinger equation. Phys Rev E 2006;74:036704.

[32] Shi B. Lattice Boltzmann simulation of nonlinear Schrödinger equation with variable coefficients. J Phys A 2010;40(33):10393.

[33] Shi BC, Guo ZL. Lattice Boltzmann model for the one-dimensional nonlinear Dirac equation. Phys Rev E 2009;79:066704.

[34] Palpacelli S, Romatschke P, Succi S. One-dimensional quantum lattice Boltzmann scheme for the nonlinear Dirac equation. Int J Mod Phys C 2013;24(12):134000.

[35] Ginzbourg I, Adler PM. Boundary flow condition analysis for the three-dimensional lattice Boltzmann model. J Phys II 1994;4:191.

[36] Ladd AJC. Numerical simulations of particulate suspensions via a discretized Boltzmann equation. Part 1. Theoretical foundation. J Fluid Mech 1994;271:285.

[37] Buick JM, Greated CA. Gravity in a lattice Boltzmann model. Phys Rev E 2000;61:5307.

[38] Guo Z, Zheng C, Shi B. Discrete lattice effects on the forcing term in the lattice Boltzmann method. Phys Rev E 2002;65:046308.

[39] Ginzburg I, Verhaeghe F, d'Humières D. Two-relaxation-time lattice Boltzman scheme: about parametrization, velocity, pressure and mixed conditions. Commun Comp Phys 2008;3:427.

[40] Silva G, Semiao V. A study on the inclusion of body forces in the lattice Boltzmann BGK equation to recover steady-state hydrodynamics. Physica A 2011;390:1085–95.

[41] Silva G, Semiao V. First- and second-order forcing expansions in a lattice Boltzmann method reproducing isothermal hydrodynamics in artificial compressibility form. J Fluid Mech 2012;698:282–303.

[42] Silva G. Discrete effects on the forcing term for the lattice Boltzmann modeling of steady hydrodynamics. Comput & Fluids 2020;203:104537.

[43] Postma B, Silva G. Force methods for the two-relaxation-times lattice Boltzmann. Phys Rev E 2020;102:063307.

[44] Yong W-A, Zhao W, Luo L-S. Theory of the lattice Boltzmann method: derivation of macroscopic equations via the Maxwell iteration. Phys Rev E 2016;93(3):033310.

[45] Suzuki K, Inamuro T, Yoshino M. Asymptotic equivalence of forcing terms in the lattice Boltzmann method within second-order accuracy. Phys Rev E 2020;102:013308.

[46] Latt J. Hydrodynamic limit of lattice Boltzmann equations (Ph.D. dissertation), University of Geneva; 2007, http://www.unige.ch/cyberdocuments/theses2007/LattJ/meta.html.

[47] Ginzburg I. Truncation errors, exact and heuristic stability analysis of two-relaxation-times lattice Boltzmann schemes for anisotropic advection-diffusion equation. Commun Comput Phys 2012;11:1439–502.

[48] Ginzburg I. Truncation effect on taylor–aris dispersion in lattice Boltzmann schemes: Accuracy towards stability. J Comput Phys 2015;299:974–1003.

[49] Qian Y-H, Zhou Y. Higher-order dynamics in lattice-based models using the chapman-enskog method. Phys Rev E 2000;61(2):2103.

[50] Silva G, Semiao V. Truncation errors and the rotational invariance of three-dimensional lattice models in the lattice Boltzmann method. J Comput Phys 2014;269:259–79.

[51] Bauer M, Silva G, Rüde U. Truncation errors of the D3Q19 lattice model for the lattice Boltzmann method. J Comput Phys 2020;405:109111.

[52] Nie X, Martys NS. Breakdown of Chapman–Enskog expansion and the anisotropic effect for lattice–Boltzmann models of porous flow. Phys Fluids 2007;19:011702.

[53] Ginzburg I. Consistent lattice Boltzmann schemes for the Brinkman model of porous flow and infinite Chapman-Enskog expansion. Phys Rev E 2008;77:066704.

[54] d'Humières D, Ginzburg I. Viscosity independent numerical errors for lattice Boltzmann models: From recurrence equations to magic collision numbers. Comput Math Appl 2009;58:823.

[55] Guo Z, Zheng C, Shi B. Force imbalance in lattice Boltzmann equation for two-phase flows. Phys Rev E 2011;83:036707.

[56] Ancona MG. Fully Lagrangian and lattice-Boltzmann methods for solving systems of conservation equations. J Comput Phys 1994;155:107–20.

[57] He X, Zou Q, Luo L-S, Dembo M. Analytical solutions of simple flows and analysis of nonslip boundary conditions for the lattice Boltzmann BGK model. J Stat Phys 1997;87:115–36.

[58] Guo Z, Zheng C. Analysis of lattice Boltzmann equation for microscale gas flows: Relaxation time, boundary condition, and Knudsen layer. Int J Comput Fluid Dyn 2008;22:465.

[59] Le G, Zhang J. Boundary slip from the immersed boundary lattice Boltzmann models. Phys Rev E 2009;79:026701.

[60] Chang H-W, Garg A, Lin C-A. Analytic solutions of the variable force effect in lattice Boltzmann methods for Poiseuille flows. Phys Fluids 2021;33:083610.

[61] Dubois F, Lallem P. Towards higher order lattice Boltzmann schemes. J Stat Mech Theory Exp 2009;2009:P06006.

[62] Holdych DJ, Noble RN, Georgiadis JG, Buckius RO. Truncation error analysis of lattice Boltzmann methods. J Comput Phys 2004;193:595–619.

[63] Zhao F. Optimal relaxation collisions for lattice Boltzmann methods. Comput Math Appl 2013;65(2):172–85.

[64] Lycett-Brown D, Luo KH. Improved forcing scheme in pseudopotential lattice Boltzmann methods for multiphase flow at arbitrarily high density ratios. Phys Rev E 2015;91:023305.

[65] Ginzburg I, Silva G, Talon L. Analysis and improvement of brinkman lattice Boltzmann schemes: bulk, boundary, interface. similarity and distinctness with finite elements in heterogeneous porous media. Phys Rev E 2015;91:023307.

[66] Yamamoto K, He X, Doolen GD. Simulation of combustion field with lattice Boltzmann method. J Stat Phys 2002;107(1–2):367–83.

[67] Chen S, Liu Z, Zhang C, He Z, Tian Z, Shi B, Zheng C. A novel coupled lattice Boltzmann model for low mach number combustion simulation. Appl Math Comput 2007;193(1):266–84.

[68] Ayodele S, Varnik F, Raabe D. Lattice Boltzmann study of pattern formation in reaction–diffusion systems. Phys Rev E 2011;83(1):016702.

[69] Lin C, Xu A, Zhang G, Li Y. Double-distribution-function discrete Boltzmann model for combustion. Combust Flame 2016;164:137–51.

[70] Hosseini SA, Darabiha N, Thévenin D. Mass-conserving advection–diffusion lattice Boltzmann model for multi-species reacting flows. Physica A 2018;499(3):40–57.

[71] Sahu A, Bhowmick S. Transient response of longitudinal fins under step changes in base temperature and heat flux using lattice Boltzmann method. J Appl Comput Mech 2022;8(3):925–39.

[72] Kuzmin A, Ginzburg I, Mohamad AA. The role of the kinetic parameter in the stability of two-relaxation-time advection–diffusion lattice Boltzmann schemes. Comput Math Appl 2011;61:3417–42.

[73] Suga S. An accurate multi-level finite difference scheme for 1D diffusion equations derived from the lattice Boltzmann method. J Stat Phys 2010;140:494–503.

[74] Straka R, Sharma KV. An accuracy analysis of the cascaded lattice Boltzmann method for the 1D advection-diffusion equation. Comput Methods Mater Sci 2020;20(4):173–84.

[75] Lin Y, Hong N, Shi B, Chai Z. Multiple-relaxation-time lattice Boltzmann model-based four-level finite-difference scheme for one-dimensional diffusion equations. Phys Rev E 2021;104:015312.

[76] Silva G, Ginzburg I. The permeability and quality of velocity field in a square array of solid and permeable cylindrical obstacles with the TRT–LBM and FEM Brinkman schemes. C R Méc 2015;343:545–58.

[77] Ginzburg I, d'Humières D. Local second-order boundary method for lattice Botlzmann models. J Stat Phys 1996;64:927–71.

[78] Silva G, Ginzburg I. Reviving the local second-order boundary approach within the two-relaxation-time lattice Boltzmann modelling. Phil Trans R Soc A 2020;378:20190404.

[79] Ginzburg I, Silva G. Mass-balance and locality versus accuracy with the new boundary and interface- conjugate approaches in advection-diffusion lattice Boltzmann method. Phys Fluids 2021;33(5):57104.

[80] Thomas JW. Numerical partial differential equations. Finite difference methods. 2nd ed.. Springer; 1995.

[81] Ganzha VG, Vorozhtsov EV. Numerical solutions for partial differential equations: problem solving using mathematica. CRC Press; 1996.

[82] Gustaffson B, Kreiss H-O, Sundstrøm A. Stability theory of difference approximations for initial boundary value problems: II. Math Comp 1972;26:649–86.

[83] Mikheev A, Krivovichev GV. Stability analysis of the lattice Boltzmann schemes with body force action. J Phys: Conf Ser 2018;1038:012040.

[84] Krivovichev GV. Stability analysis of body force action models used in the single-relaxation-time single-phase lattice Boltzmann method. Appl Math Comput 2019;348:25–41.

[85] De Rosis A. Modeling epidemics by the lattice Boltzmann method. Phys Rev E 2020;102:023301.

[86] Gantmacher FR. Applications of the theory of matrices. New York: Interscience Publishers; 1959.

[87] Miller JH. On the location of zeros of certain classes of polynomials with applications to numerical analysis. J Inst Math Appl 1971;8:397.